Parallax Modelling of OGLE Microlensing Events

Elias Waagaard
Bromangymnasiet

With support from
Dr. Rosanne Di Stefano
Department of High Energy Physics
Harvard-Smithsonian Center for Astrophysics

Initially a project in the frame of
Research Science Institute
Massachusetts Institute of Technology
May 1, 2017

Abstract

Gravitational microlensing proves to be a powerful tool to identify and estimate the properties of the lens-source system. We present a study using microlensing event data from the Optical Gravitational Lensing Experiment (OGLE), recorded in the period 2002-2016 and mainly being comprised of long events from the Galactic bulge. Our two algorithms are based on the standard point-source-point-lens (PSPL) model, and on the less conventional parallax model respectively. The optimal fit was found for each sample event in the χ^2/ν-optimization algorithm, along with the best fit parameters. Out of the 7 best fits, 4 show strong parallax effect. The microlensing fit parameters are then used with proper motion data from the Naval Observatory Merged Astrometric Dataset (NOMAD), associated to each event in order to obtain lens mass estimation for four events. These were estimated to 0.447 $M_\odot$, 0.269 $M_\odot$, 0.269 $M_\odot$ and 17.075 $M_\odot$ respectively. All masses were within the microlensing mass interval for lenses found in previous studies on this topic. In this study, we conclude that the parallax model in many cases better describe long events and demonstrate the importance of utilizing both PSPL fits and parallax fits, instead of only the PSPL model. By varying only 2 of the 7 parallax microlensing parameters instead of all simultaneously, we obtain plausible values for lens direction θ and lens transverse velocity $\tilde{v}$: a method to investigate microlensing lens properties with no regard to its luminosity. In addition, we also present spectral classes of the NOMAD objects associated with each event, which is vital for future investigations to further confirm mass estimations. We present strategies to further enhance the algorithm to analyze the microlensing event light curve to better find deviations. We also conclude that our double model can potentially unveil the presence of dim lens objects (MACHOs) such as brown dwarfs, exoplanets or black holes.

Keywords

Gravitational microlensing, Lens, Source, Einstein ring, Einstein angle, Proper motion, Transverse velocity, Galactic Bulge, Parallax, MACHO.

Contents

1 Introduction

Gravitational microlensing is today a commonly accepted method to probe the existence and behavior of Galactic objects, unbiased by their brightness. Thus, this is an accepted technique for detecting extrasolar planets, with tens of confirmed cases until this day (Rajpaul, 2012) [1]. Standard microlensing surveys like the Optical Gravitational Lensing Experiment (OGLE) utilize the Point-Source-Point-Lens (PSPL) model to a large extent for the mapping of such objects (Udalski, 2004) [2]. In order to accurately describe the gravitational microlensing light curve, comprehensive models are essential to take all the parameters into account. In this study, we present two gravitational microlensing algorithms developed to describe longer microlensing events: one using the conventional PSPL model parameters and one also taking into account the parallax effect caused by the orbital motion of the Earth, adding two more parameters. The parallax effect has only been fully detected in a handful of microlensing events, principally of long duration.

In most cases, the lens object has a luminosity of its own, which allows it to be observed and identified with conventional methods. However, this study also brings up alternative but more rare causes to gravitational microlensing: dim bodies of matter, collectively known as massive compact halo objects (MACHOs), including brown dwarfs, neutron stars and black holes. As of today, there is clear evidence that abundant quantities of unseen matter surround galaxies, as well as the Milky Way. MACHOs in the Galactic halo are even thought to be three times more massive than the visible disc and constitute several candidates for gravitational microlensing, according to Alcock (1993) [3]. Consequently, gravitational microlensing may provide an effective method for better identifying such dim objects where conventional photon-based observations falter, as they emit no or little light.

2 Background

The theory of general relativity states that massive bodies will warp the fabric of space-time. Photons of any frequency, emitted from a background source star, that travel in the regions of curvature in space-time will experience a distortion in their geodesic propagation path [1]. If a massive foreground object (the lens) passes in front of the background source star, the light will inevitably be deflected towards the observer, as illustrated in Figure (1), causing multiple distorted images of the source star. This phenomenon is called gravitational lensing. The first empirical observation to confirm this theory was done in 1919 by Sir Arthur Eddington, and quantified by Albert Einstein in 1936.

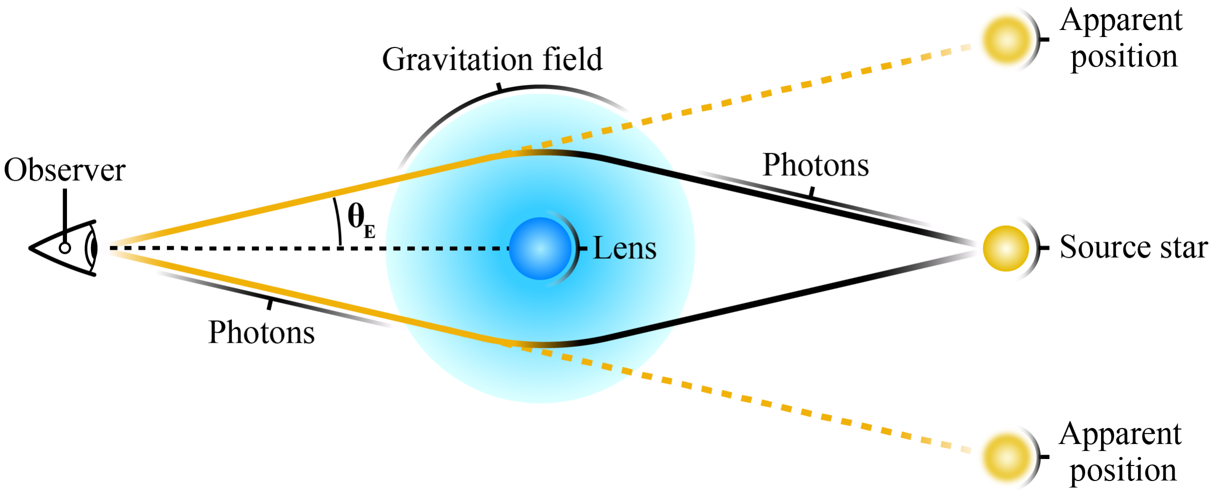

Figure 1: Deflection of light due to the massive lens.

The more massive the lens, the heavier the distortion and gravitational lensing effect will be. The number and the shape of these distorted images are a direct result of the mass distribution and the configuration of the gravitational lensing system (relative position of observer, lens and source). If the light travels in n ($n \geq 2$) paths around a single-mass lens, the observer will behold n images of the projected source star. With a sufficient number of images, the gravitational lensing will provoke a halo-shaped optical illusion as seen in Figure (2) of the light source, known as an Einstein ring.

2.1 Gravitational lensing

A common denominator for gravitational lensing is, as stated, that light from a distant background source is distorted around a foreground deflector (the lens) towards the observer. In strong gravitational lensing, the formation of Einstein rings and multiple lensed

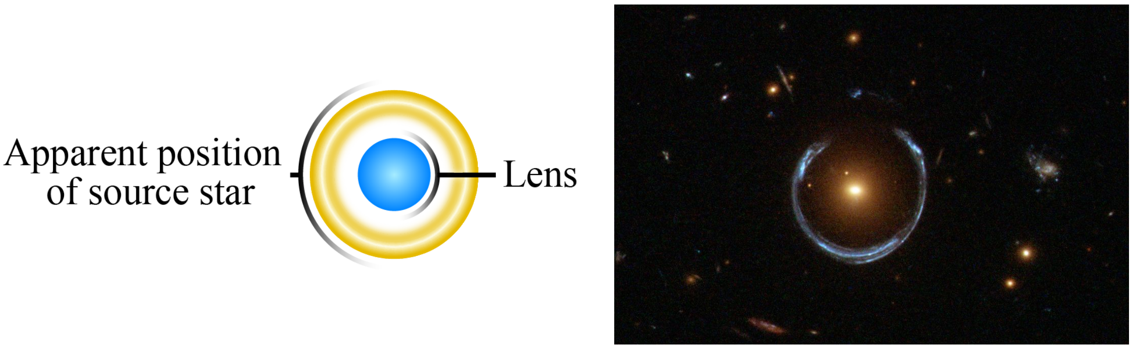

Figure 2: Left: Theoretical conception of Einstein ring around the lens from the observer's point of view. Right: A deep space image taken by the Hubble Space Telescope gives empirical evidence of the Einstein ring's existence. Image source: NASA [4]

images of a single light source easily occurs due to the satisfaction of the critical lens mass. Thus, the Einstein ring formed by a single light source can often be clearly observed, as seen in Figure (2). Weak lensing, on the other hand, distorts background light to a much smaller extent and a large number of sources is required to statistically confirm the lensing, providing a useful tool for mapping the mass distribution of clusters of dark matter. These methods have even been combined with successful outcome in surveys mapping the mass distribution of galaxy clusters (Limousin, 2007) [5].

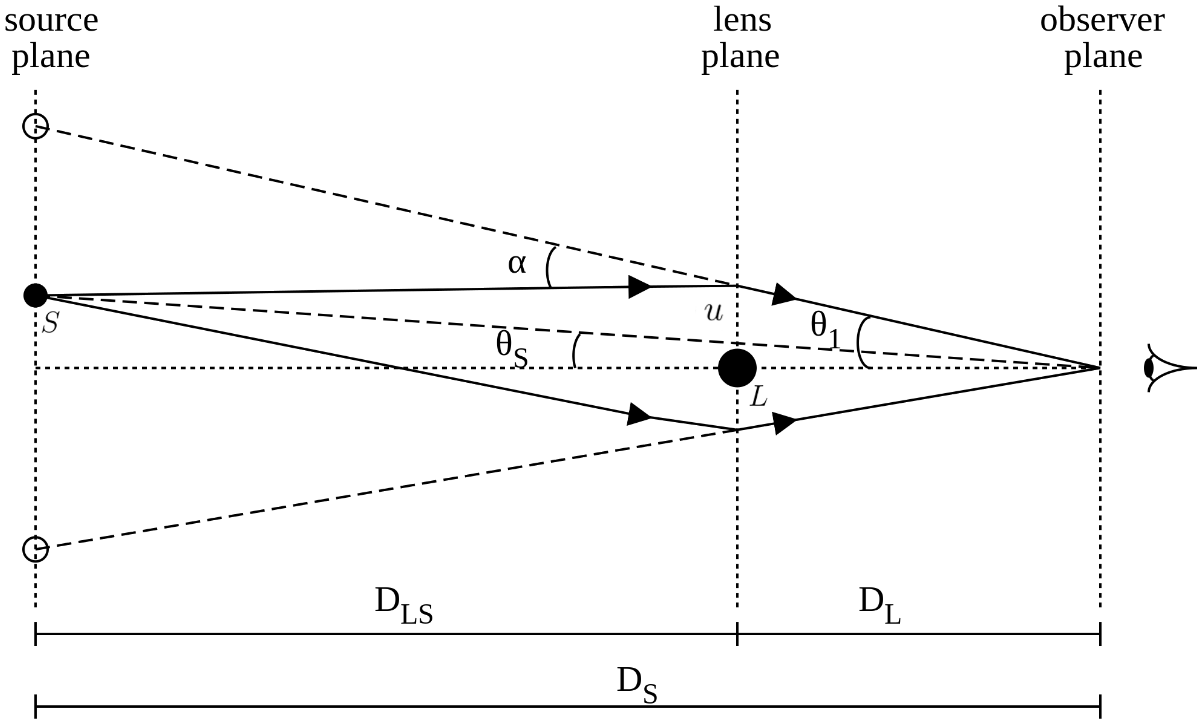

Figure 3: Gravitational Lens Geometry. Source: Krishnavedala, Wikimedia Commons

In Figure (3), the geometry of a typical gravitational lensing system is illustrated. D_S, D_L and D_{LS} describe the distance observer-source, the distance observer-lens and the distance source-lens respectively. In respect to the horizontal observer-lens plane, θ_S is the actual angle subtended by the source at the observer without lensing effect, θ_1 is the observed angle (due to gravitational lensing) subtended by the source at the observer, whereas α is the bending angle. The angular distance of closest approach, u_0, constitutes the impact parameter of the lensing effect and the magnitude at which the Einstein ring will be formed.

The mathematical components of typical point-source-point-lens microlensing events are described in detail by Paczynski et al. (1996) [6]. With values of θ_S, θ_1 and α small enough, the position of the apparent and real position of the source can be incorporated in the lens equations, along with the lens-source distance relations

$$\theta_1 D_S = \theta_S D_S + \alpha D_{LS} \tag{1}$$

$$D_{LS} = D_S - D_L. \tag{2}$$

A consequence of the general relativity would lead to a deflection of the light ray by the angle

$$\alpha = \frac{4GL}{c^2 u}, \tag{3}$$

where L is the lens mass, G is the gravitational constant, c is the speed of light and u is angular distance from the lens to the source. At a perfect alignment of the lens and the source star at the observer's location, an Einstein ring will form around the source star, featuring the Einstein angle, $\theta_{+,-}$

$$\theta_{+,-} = \frac{1}{2}\left(\theta_S \pm \sqrt{\theta_S^2 + 4\theta_E^2}\right) \tag{4}$$

The two solutions correspond to the two images of the same source S, located at opposite sides of the lens position L, at the angular distances θ_+/D_L and θ_-/D_L respectively. The angular Einstein radius θ_E (in radians) is derived from

$$\theta_E = \sqrt{\frac{4GM_L}{c^2}\frac{(D_S - D_L)}{D_S D_L}} \tag{5}$$

where M_L is the mass of the lens. The radius of the ring R_E, the Einstein radius, is the product of the angular Einstein radius θ_E and the distance to the lens D_L. The impact parameter u (angular distance source-lens) is derived from the Einstein radius

$$u = \frac{\theta_S}{R_E}. \tag{6}$$

2.2 Microlensing

A special type of gravitational lensing is microlensing, which involves detection and synthesis of the unresolved micro-images from the deflected light rays of the source into a complete macro-image, constituting the microlensing event light curve [6]. In microlensing, the size of the lens is simply dwarfed by the distance scale of the lensing system, whose Einstein ring only appears as a characteristic magnification in the light curve. Such a light curve has the advantages of being symmetric and achromatic (not dependent on the emitted source wavelength). Many microlensing searches have been initiated for the past few decades, such as EROS (Aubourg et al. 1993), MACHO (Alcock et al. 1993) and OGLE (Udalski 1992). Thanks to the high quality images of the various generations of OGLE Early Warning System (EWS), the variations of the source star flux (the received light) can be easily detected and described as a function of time. In such cases where the background light source is situated nearer the observer (smaller D_S), variability or binarity signatures of the source star itself may be large enough to manifest themselves in lensing event light curve. Di Stefano at The Harvard-Smithsonian Center for Astrophysics has demonstrated that microlensing can potentially lead to an efficient way for discoveries of dimmer nearby objects, providing an alternative detection method to the currently dominating light-based observations of stars and other luminous celestial bodies [7].

In this study, the main presumption for the microlensing event model reported by

OGLE is where a point-mass source object and a point-mass lens object move at constant velocities and align. In most cases however, the lenses associated to our sample events are simply stars with their own brightness and are not dim. The search for lensing events so far have mainly focused on regions of the sky with dense background fields, where the lensing activity is the highest, such as the Galactic Bulge, the Magellanic Clouds and even the Andromeda Galaxy (M31) [7].

The purpose of this study is to fit two different microlensing models, PSPL and parallax, to observed parametric data from OGLE light curves, with the highest possible accuracy. This can ultimately reveal the presence of dim nearby massive objects with no regard to their luminosity, such as stellar systems with companion planets, brown dwarfs, or black holes.

3 Methods

The OGLE Early Warning System database catalog provides the microlensing events studied in this paper, using Difference Image Analysis (DIA) photometry. This ensures better quality photometry in dense stellar fields, such as Galactic Bulge regions, in comparison to the classical methods from profile fitting photometry [8]. We also adapted our models to fit the Heliocentric Julian Date (HJD) timescale set by OGLE for their data.

As the purpose of this study was to compare the Point-Source-Point-Lens (PSPL) and the parallax model, a primary lower bound for the event duration was set to 100 days as the parallax effect on microlensing events is negligible for shorter events, according to Bennett et al. (2002) [9]. Hence, a first reduction was made from the total number 14963 of OGLE events (as of October 18th 2016) to 718 events of $t_E > 100$ days. As described in section 3.1, a cross-matching process with known stellar proper motion catalogs was executed to provide reference information of the investigated lens objects.

To find the best fit parameters for each investigated event, both for PSPL and parallax modelling, the χ^2-optimization algorithm (developed in Python 2.7.11) was run for each microlensing candidate in the sample. Based on the fit with the χ^2/ν closest to 1, each event was classified as a PSPL or parallax event. The theoretical background of the two

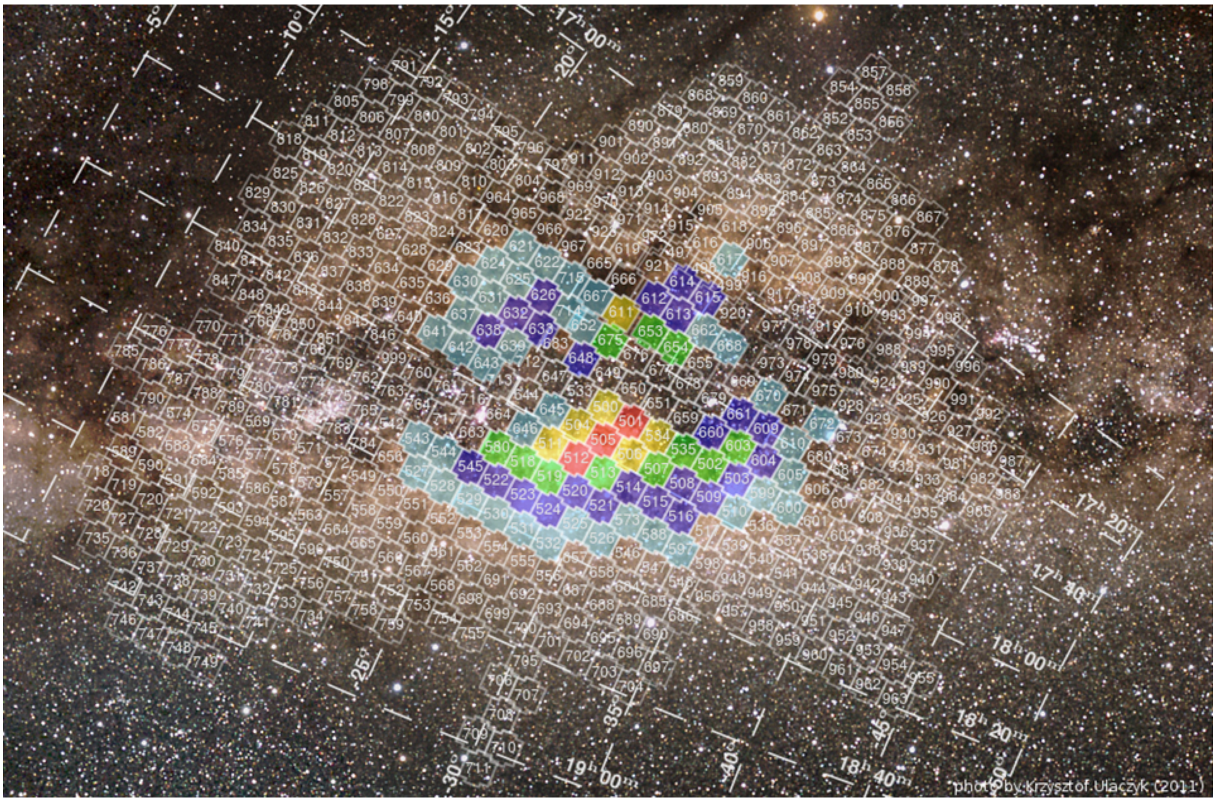

Figure 4: Map of Galactic Bulge Fields in the latest OGLE survey (OGLE IV). The grid represents equatorial coordinates in Right Ascension (RA) and Declination (Dec), and galactic coordinates in ecliptic longitude l and latitude β. The colors represent the sweep cadence (observations per night) for each field: red = 10-30, yellow = 3-10, green = 1-3, blue = 0.5-1, cyan = < 0.5, transparent = only observed occasionally. Image source: http://www.astrouw.edu.pl/ jskowron/ogle4-BLG/

algorithms are presented in detail in section 3.2 and 3.3 respectively, and are attached in Appendix B. The sample set was compiled on October 18th, 2016.

3.1 Proper Motion and Transverse Velocity Parameters

In order to find reliable background information on the investigated lens objects for this study, and thus confirming a mass or distance estimation, a cross-matching search with already known stars in the relevant particular stellar region was done. For this purpose, an important aspect to consider is the angular velocity μ, or proper motion, the apparent change in position of stars in the sky from the center of mass of the Sun

$$\mu = \frac{\theta_E}{t_E} \tag{7}$$

where θ_E is the Einstein angle and t_E is the Einstein crossing time. Altohugh most lenses have negligibly low proper motion, a sufficiently high value of proper motion enables calculation of the relative proper motion for the lens and the source, ultimately a direct measurement of the lens flux as described by Henderson et al. (2014) [10]. Therefore, if any of the investigated microlensing candidates exhibit signs of lens proper motion where $\mu \geq 8.0$ milliarcseconds per year (mas yr^{-1}), more accurate conclusions on the lensing system properties can be pulled, including spectral analysis.

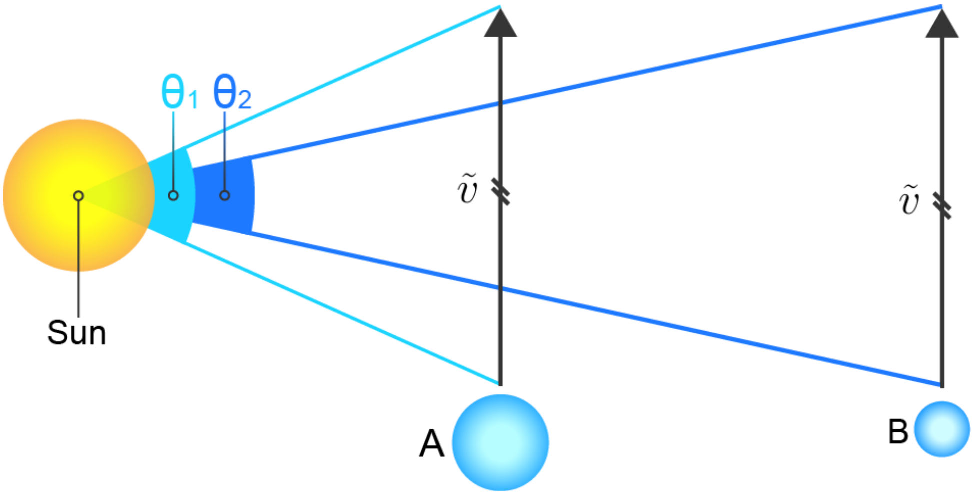

Figure 5: Illustration of proper motion from a heliocentric perspective. Despite similar transverse velocity $\tilde{v}$ ($\tilde{v}_A = \tilde{v}_B$), the closer and apparently bigger star A will have a higher proper motion than the more distant and apparently smaller star B ($\theta_1 > \theta_2$). The distance between the Sun and a given star is highly influencing its proper motion, thus also its perceived Einstein radius θ_E or its Einstein crossing time t_E, according to Equation (7).

Since the time span of the OGLE database stretches from 2002 to 2016, some microlensing systems have shifted over time due to their proper motion. Consequently, the coordinate cross-match used a search radius of 2 arcseconds (as) from where the OGLE event was reported, so that even lenses with high proper motion (100s of mas yr^{-1}) still would be tracked to their respective associated event. For this purpose, the Centre de Données astronomiques de Strasbourg (CDS) xMatch service [11] was used to compare the coordinates of the 718 OGLE events of $t_E \geq 100$ days with stars whose proper motion and spectral class were already known, cataloged in the Naval Observatory Merged Astrometric Dataset (NOMAD) [12] and provided by the VizieR cross-reference search engine [13].

The cross-matching process of lensing events and their nearby objects is done through an algorithmic matching, where the angular distance $\Delta\theta \leq 2$ arcseconds in their apparent position

$$\Delta\theta = \sqrt{(\Delta\alpha \cdot \cos\Delta\delta)^2 + \Delta\delta^2} \tag{8}$$

where α represents coordinates in right ascension (RA) and δ represents coordinates in declination (Dec). As a result, 13 OGLE events had associated stars or objects within 2 arcseconds from their apparent position.

3.1.1 Mass estimation through proper motion

However, also the proper motion of the lens plays a significant role when it comes to identifying its properties, if the lens is bright and the proper motion can be observed. On this basis, enough information can be extracted for lens mass and lens distance estimations, as seen in Equation (5). However, in this study, we resort to more suitable calculations involving proper motion and values obtained from our algorithm. According to Bennett et al. (2002) [9], the relative proper motion μ of the lens with the respect to the source can be measured to determine the lens mass with the proper motion from the NOMAD catalog and microlensing event parameters $\tilde{v}$ and θ (values obtained from the best parallax model fit described in Section 3.3), with the following formula where μ is in radians per second

$$M_L = \frac{\tilde{v} t_E^2 \mu c^2}{16G}. \tag{9}$$

Extra-galactic reference sources for proper motion measurements are not easily identified in dense stellar regions like the crowded Galactic bulge fields, acting as a complicating factor to obtain proper motion. Therefore, it can only be measured with regard to other nearby stars. However, as the source stars accounting for the OGLE events mainly reside in the Galactic Bulge, the source distance D_S is often assumed to be 8 kpc [9]: a facilitating factor to find the relative lens-source proper motion.

Consequently, this study does not only achieve analyzing each event in detail with our two algorithms but also estimating the associated lens mass.

3.2 Point-Source-Point-Lens (PSPL) Model

A well-known microlensing model, as described by Paczynski et al. (1996) [6], brings up the necessary components of a point-lens point-source microlensing system, moving at a constant transverse velocity from the geocentric plane. The magnification A, due to gravitational lensing

$$A(u(t)) = \frac{u^2 + 2}{u\sqrt{u^2 + 4}} \tag{10}$$

is proportional to the source's flux as a function of time, where a smaller lens-source angular distance u

$$u(t) = \sqrt{u_0^2 + \left(\frac{t - t_0}{t_E}\right)^2} \tag{11}$$

increases the magnification and is expressed in units of the Einstein radii θ_E. At the time of a lensing event t_0, the distance of closest approach u_0 gives the peak magnification, and t_E describes the source traversal time over the Einstein radius. The magnification is proportional to the dimensionless impact parameter u_0 (angular distance of closest approach) between the lens and the source, from the observer's line of sight. As illustrated in Figure (6), a lens trajectory closer to the source object gives a higher magnification. The lower threshold for microlensing events is generally set to maximum angular distance of $u_0 = 1$. At the event peak t_0, $u(t) = u_0$, consequently giving a net peak magnification A of $\frac{1^2+2}{1\sqrt{1^2+4}} = 1.34$ as derived from Equation (10), for lens trajectories tangent to the Einstein radius. Hence, the microlensing event duration t_E is defined when the magnification $A \geq 1.34$.

However, an important aspect to be considered for modelling microlensing events is blending of light, f_{bl}, to take the flux of other light-emitting bodies in the surroundings

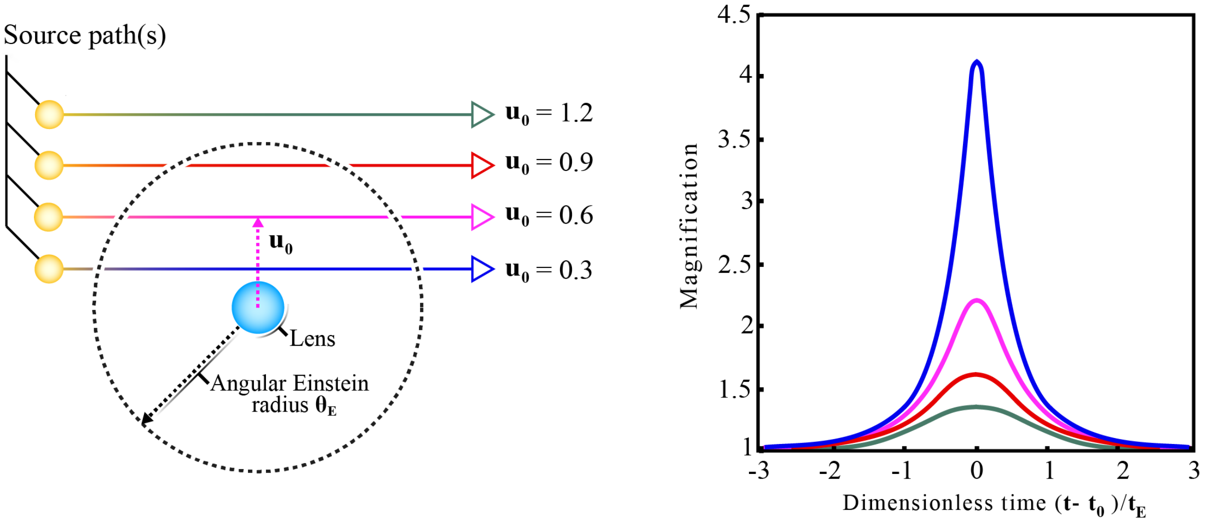

Figure 6: Lensing geometry of single-lens (PSPL) model. The typical microlensing light curves (right) are the result of various source trajectories (left), where a smaller value of impact parameter u_0 increases magnification A. t_0 marks the peak magnification of the event and t_E constitutes the duration of the magnification and therefore the length of the event.

into consideration. If there is more than one source of light along the line of sight, the magnification displays characteristics different from those of a non-blended event, with an increase in observed magnification, giving a “blended” Einstein radius (Di Stefano, 1995) [14]. The blending fraction f_{bl} expresses the proportion of flux emitted from the isolated source, given by the ratio between the apparent magnification A_{obs} and the true magnification A

$$A_{obs}(u) - 1 = (A(u) - 1)f_{bl}. \tag{12}$$

For microlensing events, the magnification appears in the I-band magnitude, the negative logarithmic brightness of star. To construct model of microlensing event light curves, the baseline magnitude I_0 for a source star is added to the I-band magnitude during the event, to reach the total visible baseline magnitude I_{bl} of a source star, including light from the lens and other light-emitting sources in the same line of sight

$$I_{bl} = -2.5\log_{10}(A_{obs}) + I_0. \tag{13}$$

This gives us yet a parameter for the PSPL microlensing event modelling. A higher blending fraction f_{bl} (low blending) would cause the light curve to appear untouched, whereas a lower f_{bl} would cause the light curve to appear compressed due to a brighter blended baseline magnitude I_{bl} in comparison to the true baseline magnitude I_0 ($I_{bl} < I_0$).

3.2.1 PSPL Model Parameters

- t_E: time required for source star to cross the Einstein radius (lower threshold for net magnification is 34 %).
- t_0: time of maximum event magnification.
- I_{bl}: observed baseline magnitude.
- u_0: minimum angular distance between lens and source from the observer's point of view, occurs at t_0.
- f_{bl}: blending fraction, the proportion of flux originating from source star.

3.3 Parallax Model

The vast majority of photmetric variation of lensing events reported by OGLE lasts around one to two months, where a change in Earth's velocity vector is too small to have an impact on the symmetric microlensing light curve. This light curve is normally modeled presuming constant velocity between the lens and the Earth-source line of sight. However, the effect of Earth's orbital motion is visible in the microlensing light of long timescale events, also called the parallax microlensing effect. This phenomenon and how to incorporate the parallax microlensing effect is described by Alcock et al.(1995) [15], who described the first observed parallax effect in gravitational microlensing, and by Bennett et al. (2002) [9].

By assuming a heliocentric perspective for a microlensing event, we simplify the parallax effect by projecting the orbital motion of the Earth along the ecliptic to the position of the lens object. In such a case, u_0 is replaced by the distance of closest approach in the Sun-source line of sight instead of the PSPL Earth-source line of sight. By generalize Equation (11) to the microlensing parallax effect, $u(t)$ is replaced by

$$\begin{aligned} u^2(t) &= u_0^2 + \omega^2(t-t_0)^2 + \alpha^2 \sin^2[\Omega(t-t_c)] \\ &+ 2\alpha \sin[\Omega(t-t_c)][\omega(t-t_c)\sin\theta + u_0\cos\theta] \\ &+ \alpha^2 \sin^2\beta \cos^2[\Omega(t-t_c)] \\ &+ 2\alpha \sin\beta \cos[\Omega(t-t_c)][\omega(t-t_c)\cos\theta - u_0 \sin\theta] \end{aligned} \tag{14}$$

where β is the ecliptic latitude and θ is the angle between the transverse velocity of the lens and the North ecliptic axis, as seen in Figure (7). t_c is the time when the Earth is at its closest point to the Sun-source line and $\omega = 2/t_E$. The parameters α and Ω are given by

$$\alpha = \frac{\omega(1\mathrm{AU})}{\tilde{v}}(1 - \epsilon\cos[\Omega_0(t-t_p)]) \tag{15}$$

and

$$\Omega(t-t_c) = \Omega_0(t-t_c) + 2\epsilon \sin[\Omega_0(t-t_p)] \tag{16}$$

where Earth's orbital eccentricity $\epsilon = 0.017$ and $\Omega_0 = 2\pi\ \mathrm{yr}^{-1}$. The lens transverse velocity $\tilde{v}$ and the lens direction θ play a crucial role for the parallax fitting. The x and y vector components of (heliocentric) transverse velocity were varied in a log-normal distribution, whose center was set to $\tilde{v} = 31.06875$ km/s with data we processed from the XHIP V/137D/XHIP catalog [16][17], as this was the mean value of all its cataloged Galactic disc objects. The relations

$$\theta = \tan^{-1}\left(\frac{\tilde{v}_y}{\tilde{v}_x}\right) \tag{17}$$

and

$$\tilde{v} = \sqrt{(\tilde{v}_x)^2 + (\tilde{v}_y)^2} \tag{18}$$

were used as additional parameters to calculate $u(t)$ for the parallax fits. These were later used as mass estimation parameters, as described in Section 4.3.1.

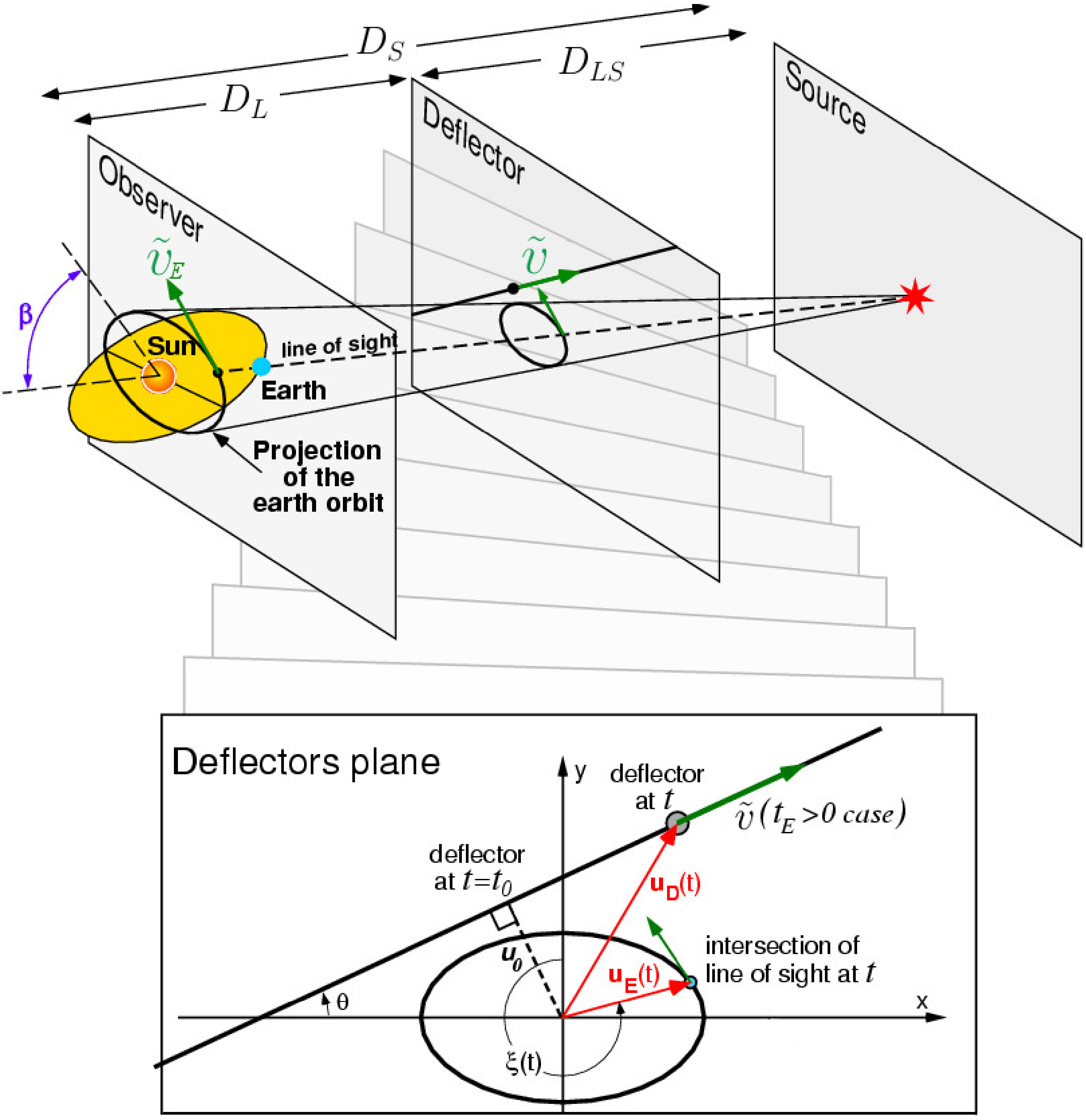

Figure 7: Geometry of parallax effect, where the point of reference is shifted from the Earth to the Sun. The Earth orbits around the Sun with a transverse velocity of v_E, whereas β is ecliptic latitude. At the deflector's plane (lower half of figure), the cross-section of the orbit of the Earth is shown as viewed on the lens plane, with regard to the lens transverse velocity $\tilde{v}$ and the lens direction θ. Image source: Rahvar et al. [18]

3.3.1 Parallax Model Parameters

- t_E: time required for source star to cross the Einstein radius (lower threshold for net magnification is 34 %).
- t_0: time of maximum event magnification.
- I_{bl}: observed baseline magnitude.
- u_0: minimum angular distance between lens and source from the observer's point of view, occurs at t_0.
- f_{bl}: blending fraction, the proportion of flux originating from source star.
- $\tilde{v}$: transverse velocity of lens projected from the position of the Sun.
- θ: angle between north ecliptic axis and the lens transverse velocity.

3.4 Chi-Square Optimization

The main input parameters for each individual event are duration t_E, angular distance u_0 of closest approach, baseline magnitude I_0, blending fraction f_{bl} and time t_0, representing the peak of the event. These five input variables are extracted from the OGLE EWS catalog [8] and are used to calculate the rate of magnification A as a function of time t. For the parallax fits, these are completed with the two additional parameters: transverse velocity $\tilde{v}$ and direction θ. Individual data points of the magnitude of the event as a function of time are plotted. We model the expected rate of magnification as a function of time according to the formula

$$I_{bl} - I_0 = -2.5 \log_{10}[A(t)], \tag{19}$$

with a fitted line in the same graph. The error margin of the observed magnitude for each data point is included in the input variables and must be included in the algorithm. The light curve model is extracted through a fitting process of a input variables from random number generator in the algorithm, which generates a large number of different values for the fit parameters. To obtain the most optimal fit with regard to the individual data points of the lensing event, the Monte Carlo method of reduced χ^2 per degree of freedom ν, was used

$$\frac{\chi^2}{\nu} = \frac{1}{n-m} \sum_{i=1}^{n} \left(\frac{I - I_i}{\sigma_i} \right)^2 \tag{20}$$

where I represents the observed magnitude, whereas I_i represents the magnitude predicted by the model. i is any given data point and n is the total number of data points. Each microlensing event reported by OGLE has a different number of data points at different magnitudes as observations are made during various amounts of available time, leading to different n for each event. σ_i stands for the standard devition, or error margin, of the observed magnitude reported by OGLE for each data point [8]. The error margin also varies for each data point, where a dim magnitude often leads to a higher uncertainty. However, an underestimated error margin ultimately leads to high values of χ^2 and undermines the perceived validity of in reality good fits. The degree of freedom ν is the number of data points n minus the number of fitted parameters m, which in our study was 5 for PSPL fits and 7 for parallax fits, as the transverse velocity $\tilde{v}$ and the angle θ were also included as parameters for the parallax model.

In order to optimize χ^2/ν, we varied each parameter within its own Gaussian distribution, choosing the official OGLE values and standard error (their expected values for the fit) as the initial center of the distribution for each parameter. The purpose of the algorithm was to generate different combinations (1000 per iteration) of the parameter values, representing one fit each. The newly generated combinations of parameters then replaced the Gaussian center if they showed a better fit than the previous ones, producing a lower value of χ^2/ν. This process was then repeated with additional iterations until there was no improvement of the χ^2/ν among the combinations in one iteration. As a result, this algorithm lead to an asymptotic improvement of the χ^2/ν until the best possible.

4 Results

As previously stated, the number of investigated microlensing events in period 2002-2016 from OGLE EWS was successively reduced in two steps. Firstly, out of the total number of 14963 events, 718 were selected based on their duration ($t_E > 100$ days) to maximize relevance for the parallax model experiments. Secondly, the equatorial coordinates of these 718 events were cross-matched with the NOMAD catalogs of stellar objects and their proper motion.

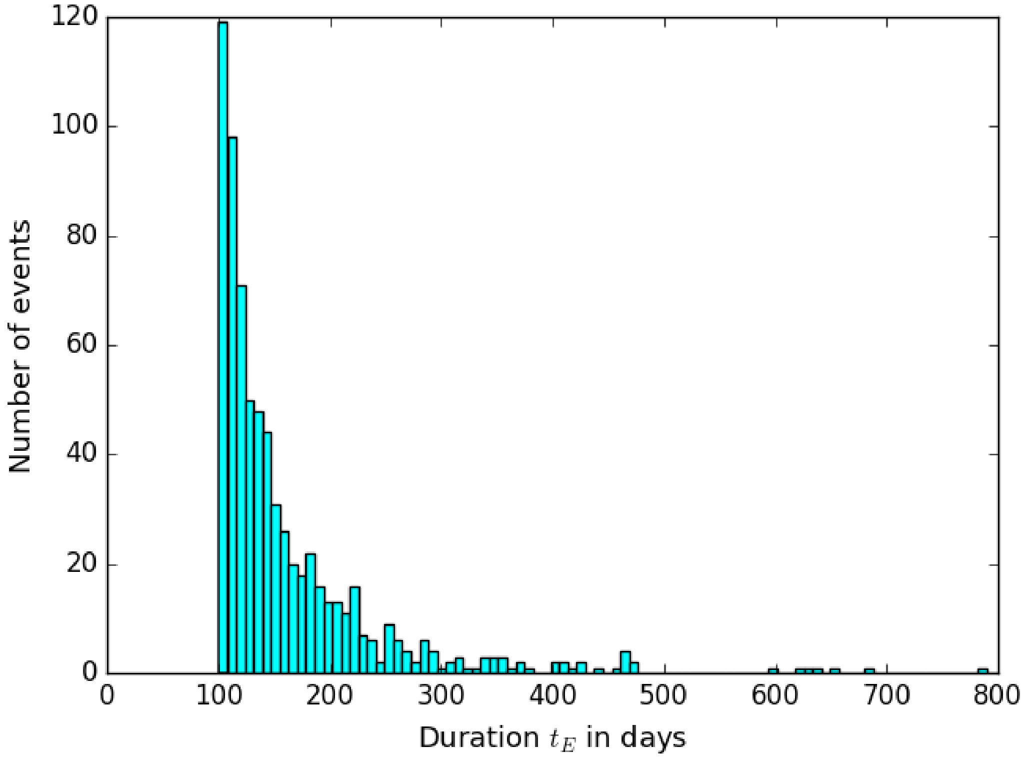

Figure 8: Histogram of t_E distribution among selected OGLE EWS events in the first sample of all OGLE events longer than 100 days. In this first sample, the shortest events close to 100 days are the most commonly occurring type.

We succeed to match and link 13 of these events to stars with known proper motion and with, to some extent, known spectral properties. This constitutes the second sample. Out of these 13 events, we found 7 events whose χ^2/ν was below our cut-off value of 3.0. Out of these, 4 events had better parallax fits and 3 events had better PSPL fits, presented in the Table (1).

Event	**Model**	t_0	t_E	I_0	u_0	f_{bl}	θ	$\tilde{v}$	χ^2/ν
2002-334	PSPL	2452698.372	172.788	16.186	0.195	0.349	–	–	8.519
	PAR	2452690.555	189.415	16.194	0.195	0.364	-0.164	108.325	11.751
2005-36	PSPL	2453539.341	176.355	18.656	0.394	0.971	–	–	2.675
	PAR	2453544.823	188.507	18.646	0.397	0.955	0.355	41.728	2.910
2006-230	PSPL	2453947.193	175.054	17.953	0.270	0.171	–	–	2.986
	PAR	2453940.415	180.177	17.930	0.265	0.147	2.309	49.449	3.164
2008-51	PSPL	2454634.078	276.396	16.444	0.367	0.059	–	–	2.186
	PAR	2454628.316	246.991	16.447	0.723	0.166	3.685	8.788	2.357
2011-64	PSPL	2455746.139	144.857	16.088	1.396	0.834	–	–	5.785
	PAR	2455757.185	160.613	16.092	1.321	0.761	1.302	38.418	5.508
2011-1349	PSPL	2455813.094	295.698	16.033	0.130	0.083	–	–	8.594
	PAR	2455814.657	268.921	16.029	0.128	0.084	-3.091	10.980	7.813
2013-1831	PSPL	2456587.812	152.938	19.145	0.692	0.947	–	–	2.065
	PAR	2456581.674	150.851	19.145	0.664	0.891	-1.212	17.107	2.064
2014-1159	PSPL	2456909.160	293.461	18.646	0.210	0.111	–	–	1.762
	PAR	2456892.394	208.140	18.639	0.285	0.156	-2.787	8.443	1.741
2015-74	PSPL	2457058.517	121.591	19.379	0.008	0.123	–	–	2.939
	PAR	2457061.988	137.106	19.364	0.013	0.066	1.991	25.290	2.877
2015-539	PSPL	2457067.723	153.288	18.342	0.077	0.260	–	–	5.795
	PAR	2457077.924	135.129	18.336	0.122	0.284	-2.252	25.613	5.508
2015-1493	PSPL	2457271.768	212.697	18.494	0.043	0.083	–	–	3.275
	PAR	2457273.797	203.494	18.503	0.063	0.110	3.014	20.483	3.387
2016-443	PSPL	2457544.591	196.500	19.204	0.020	0.595	–	–	3.209
	PAR	2457545.703	194.207	19.197	0.020	0.568	-0.677	32.904	4.616
2016-749	PSPL	2457507.971	128.553	20.447	0.008	0.174	–	–	2.662
	PAR	2457507.248	153.127	20.402	0.003	0.169	2.106	38.605	2.505

Table 1: Summary table of the optimal parameters for the PSPL and parallax (PAR) fits for each OGLE Bulge event, obtained with the chi-square optimization algorithm, where θ is in radians and $\tilde{v}$ is in kilometers per second. The respective fit with the lowest χ^2/ν for each model is presented for all of the 13 events in the final sample. Original OGLE values for the five PSPL parameters can be found in Table (3) in Appendix A, for the sake of comparison.

4.1 Parallax Fits

Shown below are the parallax and PSPL fits for OGLE-2013-BLG-1831, OGLE-2014-BLG-1159, OGLE-2015-BLG-74 and OGLE-2016-BLG-749. As the parallax fits were classified as better than the PSPL fits for these events, the occurrence of parallax effect can be confirmed with higher certainty. The baseline magnitude for these event ranges between 18.65 and 20.50, and the duration ranges between 141 and 249 days, some of the longer in the OGLE database. In addition, to obtain greater understanding of the parallax parameters, we varied only the θ and $\tilde{v}$ parameters in the χ^2/ν-optimization algorithm instead of all the seven at once. This can be seen in the color distributions below, where each point represent one fit. The values for these two parameters from the best fit and their χ^2/ν-value are presented, along with the plausible interval for them. In comparison, the χ^2/ν of the parallax fits from Bennett et al. (2002) [9] ranged from 1.20 to 2.34, being classified as good fits.

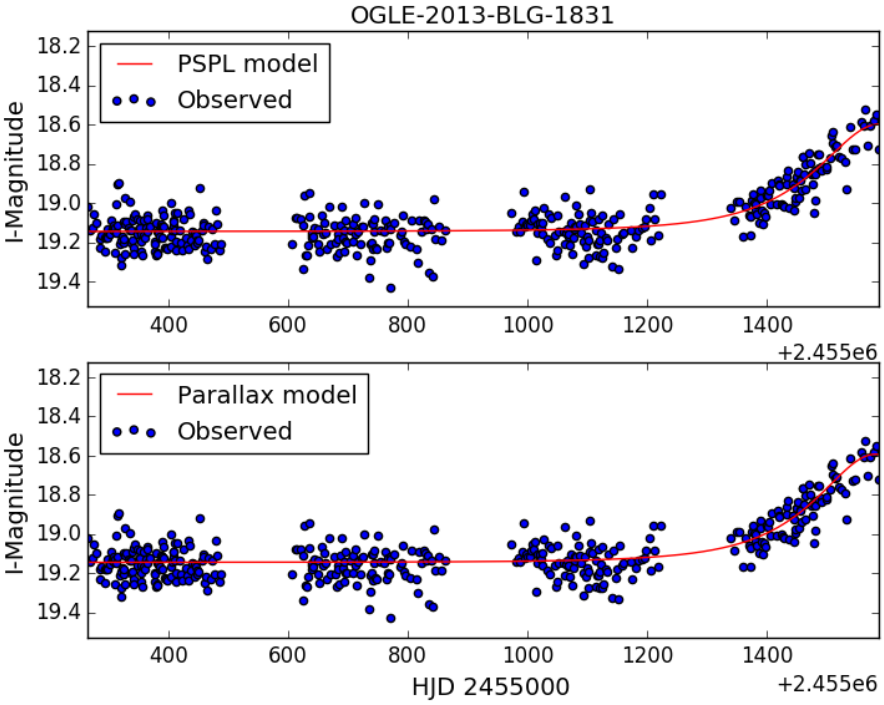

Figure 9: OGLE-2013-BLG-1831 PSPL fit ($\chi^2/\nu = 2.065$) and Parallax Fit ($\chi^2/\nu = 2.064$).

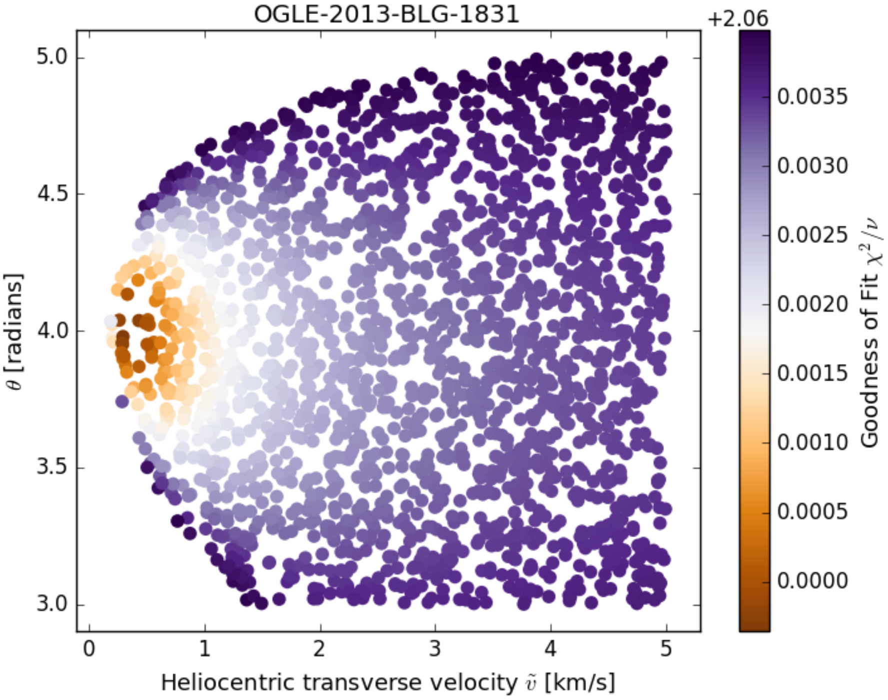

Figure 10: Distribution of plausible transverse velocity and theta values for OGLE-2013-BLG-1831. The color gradient scale shows the goodness of fit χ^2/ν, where brown represents better fits whereas blue shows subpar fits. The plausible transverse velocity ranges between 0.1 and 2.0 km/s (best solution at 0.294 km/s), and its projected direction somewhere between 3.5 and 4.5 rad (best solution at 3.979 rad).

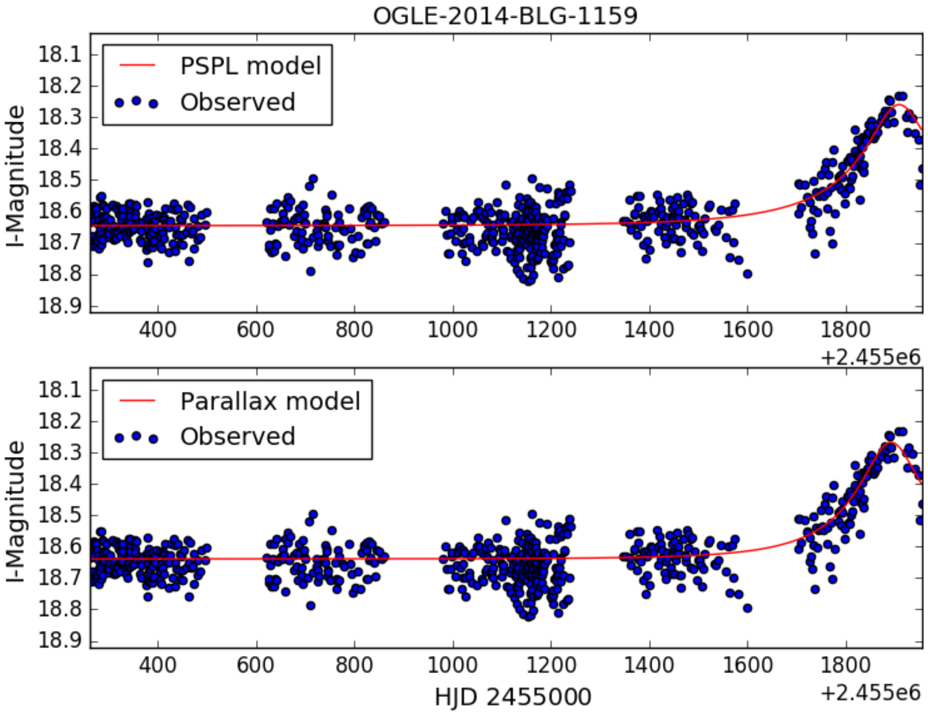

Figure 11: OGLE-2014-BLG-1159 PSPL fit ($\chi^2/\nu = 1.762$) and Parallax Fit ($\chi^2/\nu = 1.741$).

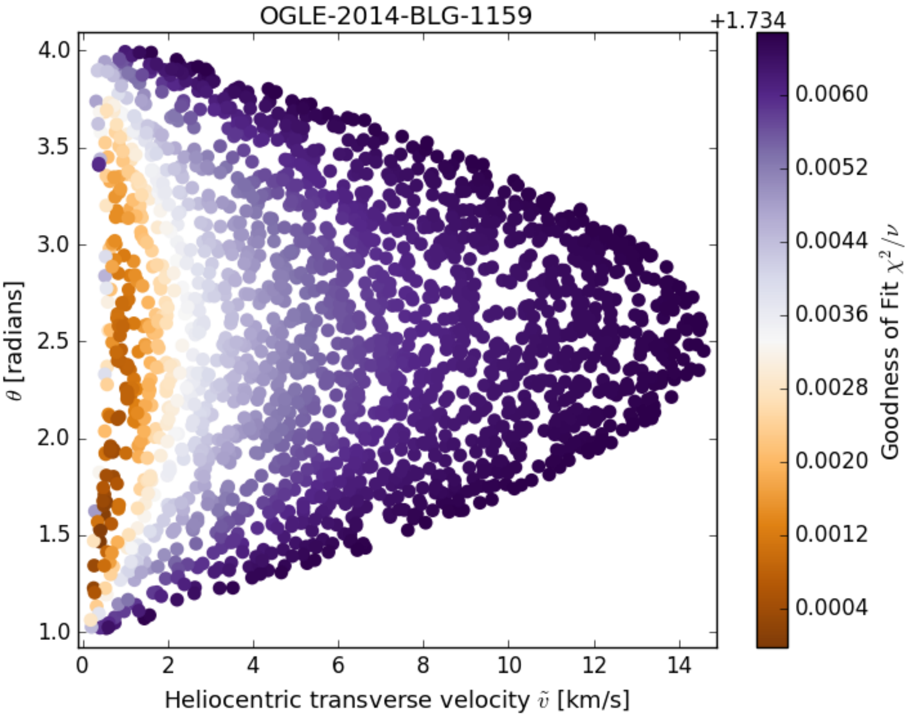

Figure 12: Distribution of plausible transverse velocity and theta values for OGLE-2014-BLG-1159. The color gradient scale shows the goodness of fit χ^2/ν, where brown represents better fits whereas blue shows subpar fits. The plausible transverse velocity ranges between 0.1 and 4.0 km/s (best solution at 0.410 km/s), and its projected direction somewhere between 1.0 and 4.0 rad (best solution at 1.734 rad).

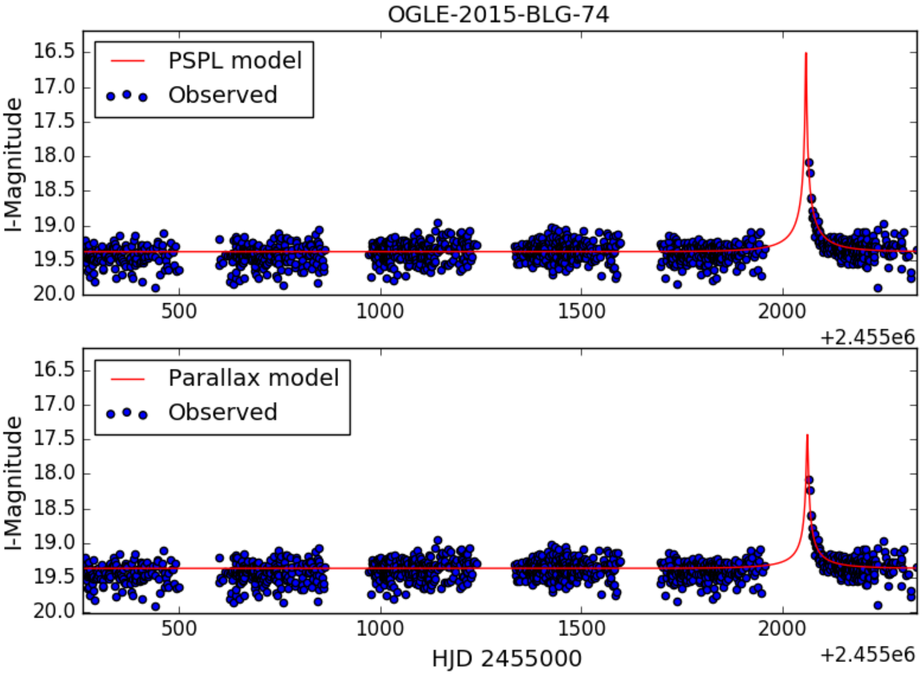

Figure 13: OGLE-2015-BLG-74 PSPL fit ($\chi^2/\nu = 2.939$) and Parallax Fit ($\chi^2/\nu = 2.877$).

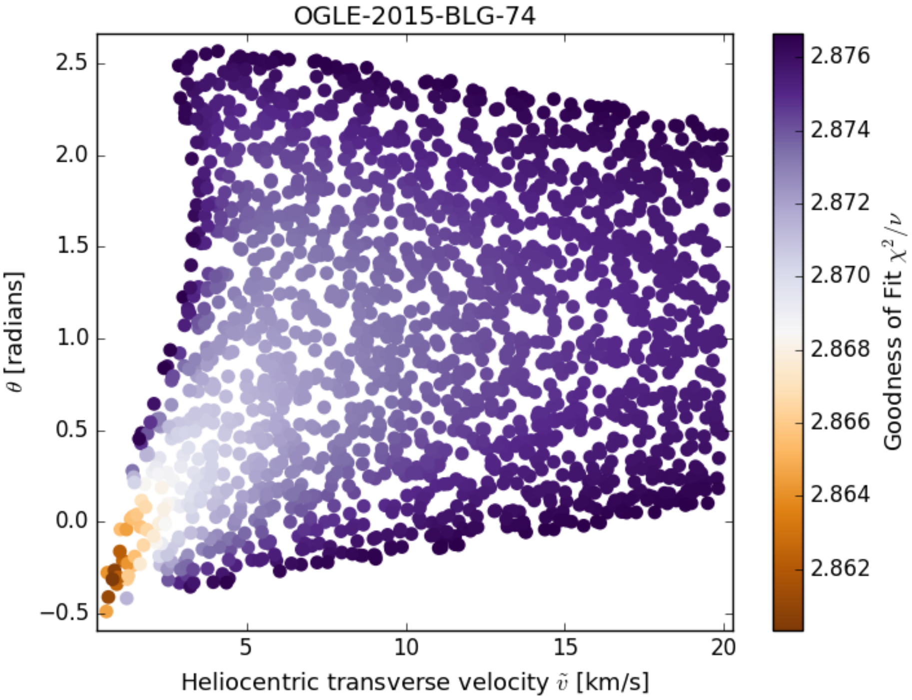

Figure 14: Distribution of plausible transverse velocity and theta values for OGLE-2015-BLG-74. The color gradient scale shows the goodness of fit χ^2/ν, where brown represents better fits whereas blue shows subpar fits. The plausible transverse velocity ranges between 0.1 and 5.0 km/s (best solution at 0.797 km/s), and its projected direction somewhere between -0.5 and 2.5 rad (best solution at -0.314 rad).

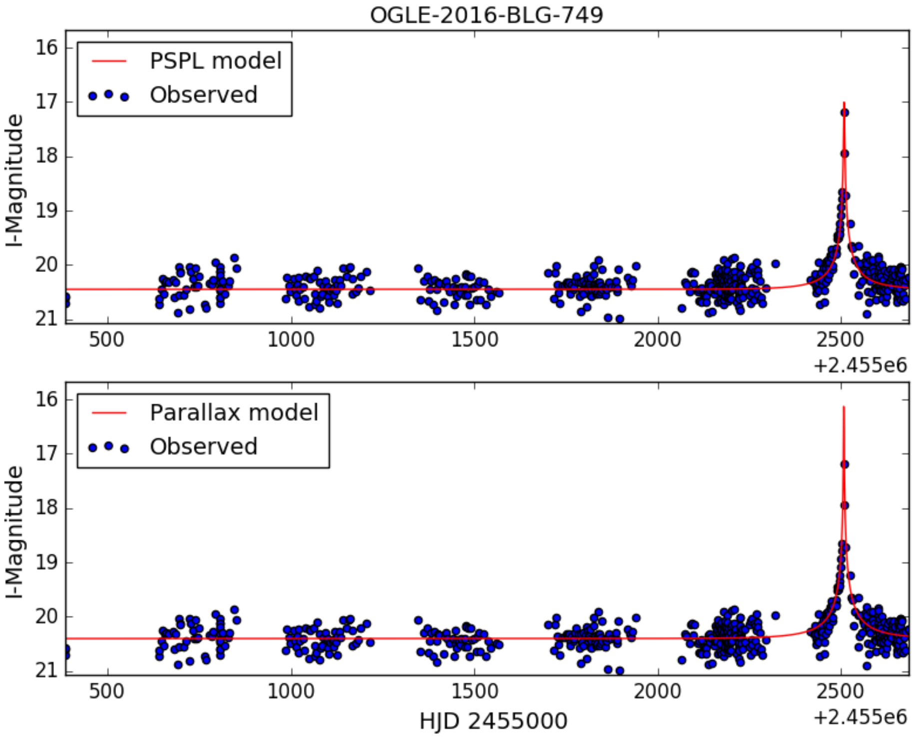

Figure 15: OGLE-2016-BLG-749 PSPL fit ($\chi^2/\nu = 2.662$) and Parallax Fit ($\chi^2/\nu = 2.505$).

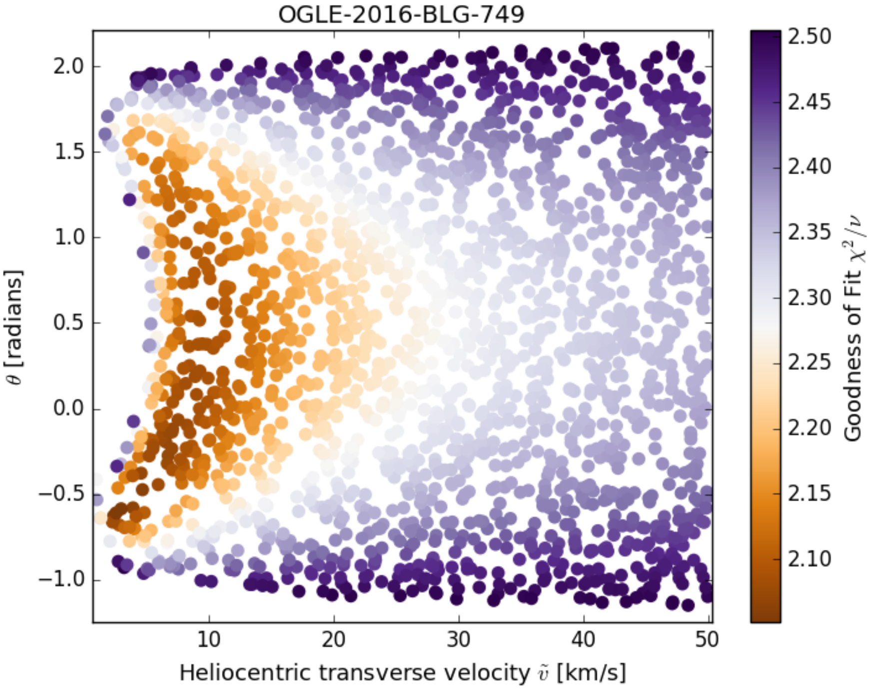

Figure 16: Distribution of plausible transverse velocity and theta values for OGLE-2016-BLG-749. The color gradient scale shows the goodness of fit χ^2/ν, where brown represents better fits whereas blue shows subpar fits. The plausible transverse velocity ranges between 0.1 and 30.0 km/s (best solution at 2.985 km/s), and its projected direction somewhere between -1.0 and 2.0 rad (best solution at -0.587 rad).

4.2 PSPL Fits

Presented below are the parallax and PSPL fits for the events OGLE-2005-BLG-36, OGLE-2006-BLG-230 and OGLE-2008-BLG-51, whose PSPL fits were better than the parallax fits. Their baseline magnitude ranges from 16.4 to 18.6, and a duration ranging from 175 to 276 days. As the PSPL model was better in this case, lens transverse velocity estimates should suffer from a slightly higher uncertainty, as the lens transverse parameter is derived from the parallax fit.

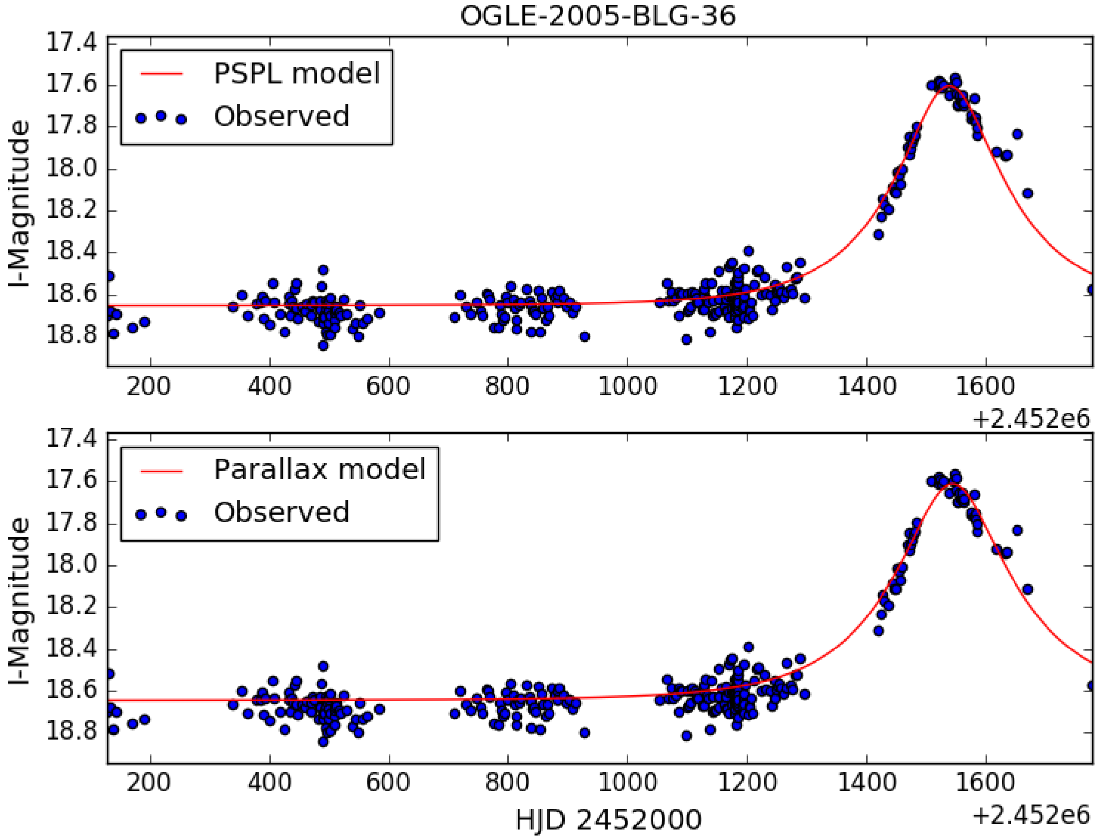

Figure 17: OGLE-2005-BLG-36 PSPL fit ($\chi^2/\nu = 2.675$) and Parallax Fit ($\chi^2/\nu = 2.910$).

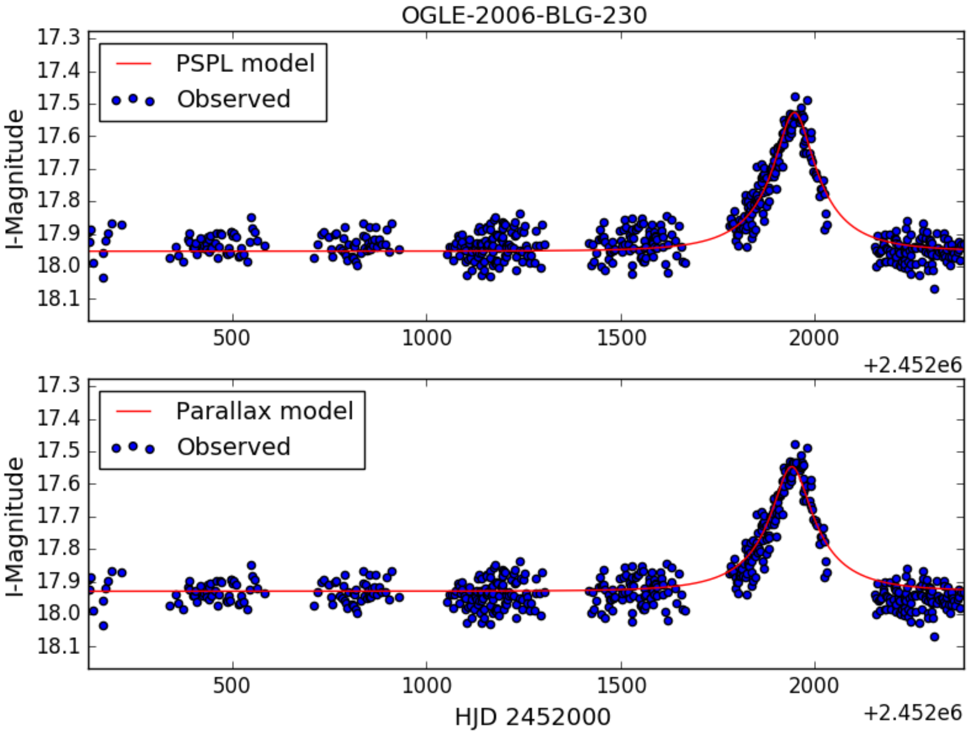

Figure 18: OGLE-2006-BLG-230 PSPL fit ($\chi^2/\nu = 2.986$) and Parallax Fit ($\chi^2/\nu = 3.164$).

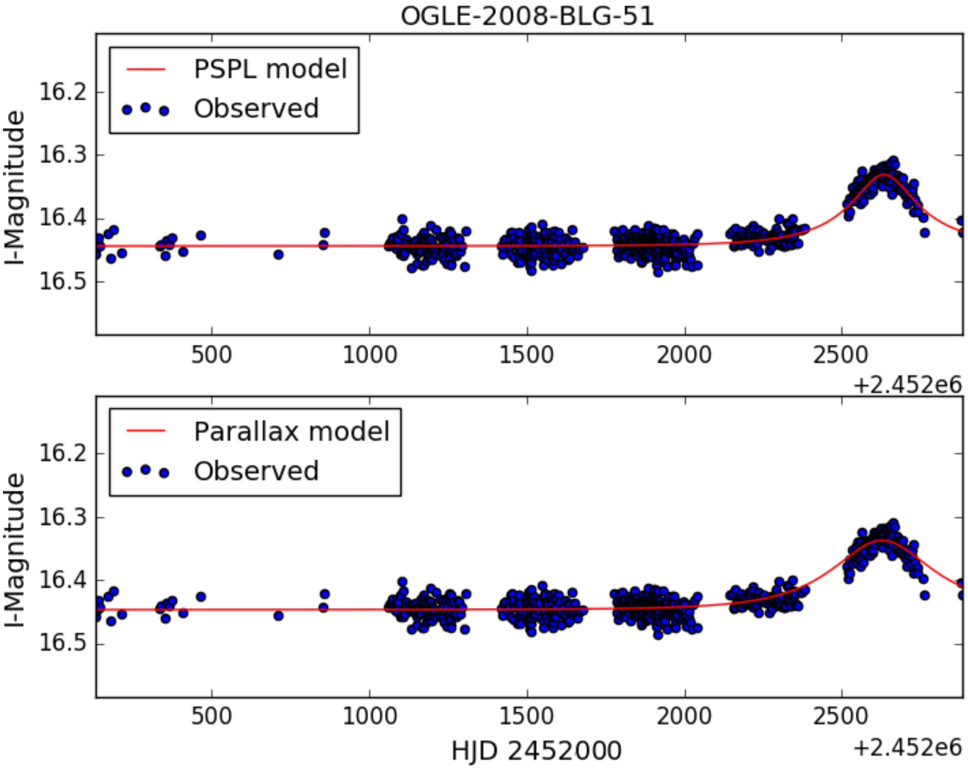

Figure 19: OGLE-2008-BLG-51 PSPL fit ($\chi^2/\nu = 2.186$) and Parallax Fit ($\chi^2/\nu = 2.357$).

4.3 Proper Motion Catalog Matching

As a consequence of stellar activity, photons of different wavelenghts are emitted. The chronomatric spectrum gives a fingerprint of background source stars and their properties. Since temperature is proportional to stellar mass, such properties can be analyzed to further improve knowledge about investigated lensing events with more ample conclusions. In the crowded Galactic Bulge where the stellar density is high and the source stars associated with OGLE events reside, most stars are old and metal-poor, of which a large fraction is classified as red giants or red dwarfs (both K and M spectral type) [19].

Associated Event	**Angular Distance (arcsec)**	**NOMAD 1.0 Survey ID**	**Bmag**	**Vmag**	**Rmag**	**Jmag**	**Hmag**	**Kmag**	**pmRA**	**pmDec**
2002-334	1.112808	1080-00344795	20.7	–	18.29	–	–	–	–	–
2005-36	1.941986	1081-00346476	17.73	–	17.46		–	–	–	–
2006-230	1.955862	1079-00370811	19.86	–	17.83	–	–	–	–	–
2008-51	1.451029	1080-00348647	20.13	–	18.17	–	–	–	–	–
2011-64	1.555922	1080-00346977	20.64	–	–	–	–	–	122	-346
2011-1349	1.342368	1075-00347489	14.87	15.4	13.78	13.903	13.518	13.41	–	–
2013-1831	1.876859	1077-00372129	17.57	16.72	15.5	14.108	13.448	13.167	–	–
2014-1159	1.65265	1082-00337229	18.21	17.95	18.17	16.783	17.454	17.155	–	–
2015-74	1.999414	1078-00378268	17.64	17.01	16.2	15.734	15.202	15.179	–	–
2015-539	1.999377	1078-00376758	20.49	–	18.23	–	–	–	18	-8
2015-1493	1.832459	1079-00367145	20.07	–	17.58	–	–	–	2	-4
2016-443	1.736238	1078-00376041	20.62	–	18.31	–	–	–	-2	4
2016-749	0.896991	1077-00368708	20.41	–	20.04	–	–	–	–	–

Table 2: Summary table of the results from the cross-matching process between the OGLE microlensing event from the final sample and objects from the NOMAD Survey Catalog [12], using the CDS Xmatch Service [11]. The data belonging to the respective NOMAD objects is presented along with its associated OGLE event and the respective angular distance from the match. These were matched within a search radius of < 2 arcseconds. The proper motion μ (with vector components in RA and Dec) are measured in milliarcseconds/year (mas yr^{-1}). Note that only event (2011-64) is associated with a high proper motion object, and only another three events associated with objects where μ was known (2015-1493, 2016-443 and 2016-749).

4.3.1 Lens mass estimation

In order to get an estimate of the lens mass, one can either resort to spectral analysis based on the classes of the lens candidates listed above, or even better, to mass estimation with proper motion as seen in Equation (9). For the latter, the transverse velocity $\tilde{v}$ and duration t_E from the best parallax fit from the respective events were utilized.

Out of these four events with a matched NOMAD object whose proper motion μ was known, we assumed for the sake of simplicity that the object relates to the lens, due to the shorter distance from the observer. This distance relation implies a higher μ for the lens, whereas the source would in such case have a negligibly small μ in comparison. Based on this presumption, the by NOMAD observed μ was therefore set as the relative proper motion between the lens and the source.

Our calculations estimated that the lens mass for 2015-539 was 0.447 $M_\odot$, that the lens mass for 2015-1493 was 0.269 $M_\odot$ and that the lens mass for 2016-443 also was 0.269 $M_\odot$. Despite a spiking proper motion value associated with the event, the lens mass 2011-64 was estimated to 17.075 $M_\odot$ but was not ruled out as a realistic Galactic disc lens mass. Confirmation of its validity can be found in mass estimations for similar events conducted by Alcock (1995) [15] and Bennett (2002) [9] using a different method, the so-called distance-mass likelihood function, that gave values within the similar mass interval as our study based on proper motion. For instance, Bennett acquires lens mass estimations ranging from 0.33 $M_\odot$ to 6 $M_\odot$, with a mean of 2.7 $M_\odot$. Considering the vast numbers of possible lens objects of various mass in the Galactic disc, we conclude that this accordance is an indicator of accurate lens mass estimations in our study.

5 Discussion

With this study, we demonstrated the importance of performing both parallax and PSPL fitting for long microlensing events, as well as the importance of the derived parameters from the best model fits, such as transverse velocity. In most cases, we obtained good fits of seemingly similar or better quality to the fits made by OGLE for the same events. Since there are no official values of χ^2/ν for the OGLE fits, we chose their official values of the five PSPL parameters for each event as initial algorithmic values for our fits. Thus, we decided to set the cut-off value for our χ^2/ν to 3, which may seem relatively high with regard to standardized accepted values, which are supposed to be close to 1. However, since the focus was to compare our two models, we considered the relative error between different fits more relevant than the absolute error of each event. Another possible reason for high χ^2/ν might be that the official error variance σ_i provided by OGLE for each data point in each event probably suffers from systematic underestimation and is simply too low, which would naturally lead to a higher χ^2/ν despite a seemingly good fit. This is especially relevant for our study, as it comprises OGLE events of very dim magnitude with already high uncertainty for each data point, potentially even higher than reported. For future studies, the error variance would be tested further and readjusted accordingly. In addition, the fact that the χ^2/ν-intervals for the parallax fits in Bennett's study also were similar to ours is yet another indicator of the precision of our models.

Nonetheless, optimizing our algorithms and model fits to obtain lower χ^2/ν-values may prove to be an important step leading to further discoveries. For instance, analyzing light curve irregularities can potentially reveal the presence of exoplanets with no intrinsic luminosity orbiting around the lens star, typically lasting for a few hours or a few days. Consequently, these relatively small light curve deviations often need verification from multiple sources. A prime example of the discovery of a multiple-planet system through gravitational lensing is the event OGLE-2006-BLG-209, where the existence of two gas giants could be confirmed through a combined effort from not only the OGLE survey but also from MOA, MicroFUN and PLANET/RoboNET [20].

However, these light curves irregularities similar to ones caused by the orbital motion of the Earth may in some cases be an effect of binary stellar systems, the so-called "xallarap" effect ("parallax" spelled backwards). This is also described by Bennett (2002) [9] as the phenomenon when the intrinsic orbital motion of binary stellar system makes the light curve resemble to the normal parallax effect: Earth-mimicking period, inclination, eccentricity and phase. A χ^2/ν-threshold for parallax fits partly eliminates this problem and helps to clearly distinguish between the two models, according to Bennett, which our method includes (where $\chi^2/\nu \leq 3.0$). This is also something that with additional research could potentially be incorporated in the algorithm as a third model, and potentially differentiate properly between the microlensing parallax effect and binarity. With this in mind, our two combined algorithms proved successful to give a more complete view rather than only employing the standardized PSPL model, as used by major microlensing services like OGLE.

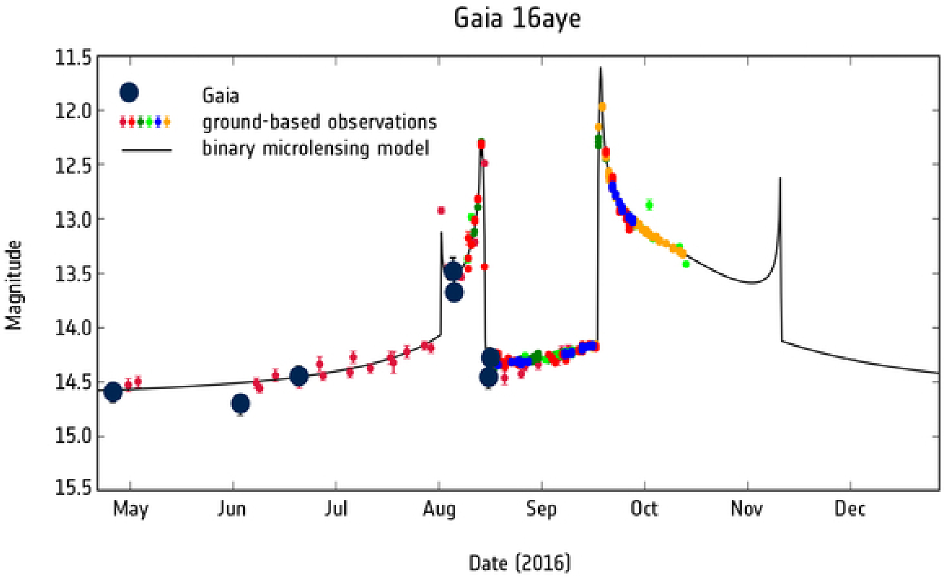

Figure 20: Example of a gravitational microlensing light curve affected by the intrinsic orbital motion of a binary stellar system, resulting in varying brightness and significant peaks. The binary model was developed by scientists at the European Space Agency (ESA) and relies on data from the GAIA satellite, also speculating about the presence of planets in orbit or a black hole. In the future, we want to develop a similar binary model for this type of microlensing events, acting as an extension to the already existing PSPL and parallax models. Image source: http://sci.esa.int/gaia/58547-light-curve-of-binary-microlensing-event-detected-by-gaia/.

The transverse velocity of the lens was obtained for all the 13 sample events, but confirmed with higher certainty for the 4 events with the best parallax fits. In addition to fits, we performed distributions of varied values of the lens direction θ and the lens transverse velocity $\tilde{v}$. By varying these two parameters only, these distributions gave us a better and more accurate picture of plausible values for the lens direction and transverse velocity, rather than only performing parallax fits where we varied all the 7 parameters at the same time. The general trend showed a lower lens transverse velocity for our sample events than the average Galactic disc transverse velocity, from the XHIP catalog. This is probably due to the fact that long events often imply low transverse velocity, which would also give small proper motion. This is a very relevant remark, since this study dealt with some of the longest events in the whole OGLE database.

For future studies, we would search for more photometric information associated with the sample events and analyze the relative proper motion between the lens and the source more deeply. In this study, only 4 events were linked to objects with verified proper motion (those with an estimated lens mass). We supposed that the NOMAD data corresponds to lens proper motion and not to the source, due to the closer distance and thus normally a higher proper motion that can be recorded. To ensure this assumption, additional catalogs and studies would need to be consulted to properly differentiate between lens and source proper motion, and ultimately find the relative proper motion.

An explanation for the the absence of known proper motion associated to OGLE events might be that the lens itself is a dimmer object with low luminosity, a so-called MACHO (massive compact halo object). In the Galactic Bugle, MACHOs are frequently occurring, albeit at a relatively low percentage of the total amount of objects. According to Gould (2005) [21], MACHOs are the cause of 1.2 % of the lensing events from the Galactic Bulge. The low probability of MACHOs indicates that further catalog cross-matching is necessary to associate lenses of OGLE events to cataloged objects, but is relevant nonetheless. In the case of such a non-luminous lens, it would not be possible to find proper motion data from catalogs such as NOMAD, according to Gould. In extreme cases, MACHOs might be the case for a few of our sample events. Through further spectral analysis and also alternative mass estimations such as the distance-mass likelihood function, this interesting track might even lead to the discovery of a dim stellar remnant (black hole or neutron star) acting as the lens.

Moreover, although mass estimations were not the main focus of our study, we used the mass equation from Bennett (2002) for the four events with associated proper motion that we selected. They all gave realistic lens masses within the mass interval for Galactic disc lenses, an indicator of the equation's effectiveness and compatibility with our study. Despite the fact that both Bennett and Alcock (1995) used a different method for lens mass and distance estimations (the distance-mass likelihood function), we obtained lens masses in similar intervals. However, the comprehensive method presented in this study, of combining both PSPL and parallax fitting with matched proper motion data, has not to our knowledge been performed to this extent in other studies. An advantage with lens mass estimations based on proper motion, used in our study, is that relative proper motion can be measured very accurately even years after the event. In addition, proper motion observations have lower uncertainty than those of transverse velocity, according to Bennett. Consequently, further research in proper motion and cross-checking with these alternative methods would allow us to determine lens mass intervals even more accurately.

6 Conclusion

To conclude, we showed that by using these two models for longer gravitational microlensing events, instead of a single PSPL one as used by OGLE, we provided a helpful tool to even more accurately describe this manifestation of Einstein's general theory of relativity. As the parallax effect in gravitational microlensing is relatively unexplored, whose presence only has been officially reported in a handful of microlensing events, we demonstrated the importance of performing both models as well as some candidate events with strong parallax effect. We also achieved an improvement of the understanding of this phenomenon by finding the best possible event parameters for each event in our algorithm, in some cases different to those published by OGLE. In addition, our model fits are an indirect way to measure lens mass and ultimately lens distance through associated proper motion data, which is normally considered difficult in astronomy, especially for dim objects. Furthermore, we concluded that this method even has the potential to discover non-luminous lenses, such as exoplanets and black holes, which otherwise hardly reveal their presence.

7 Acknowledgments

I deeply thank Dr. Rosanne Di Stefano for initially catching my attention in this exciting field of microlensing, having inspired me to undertake a project in this field. I express gratitude to the Center for Exellence in Education and to the Massachusetts Institute of Technology (MIT) for making the enriching and life-changing Research Science Institute (RSI) experience come true, and to Young Scientists for invaluable sponsorship that enabled me to participate. I thank Bromangymnasiet, Hudiksvall, for sponsoring me and believing in my project. I thank my fellow Rickoid and lab partner Lia Eggleston for her fantastic support, for her hardworking spirit and her precious expertise in computing, without whom I would never have reached as far. I want to thank my lab collegues Sarayu Narayan and Dang Pham at Harvard for their useful advice and support in the jungle of programming. In addition, I want to thank Dr. John Rickert for strong support and tutorship, having spent hours proofreading. I want to thank Louise Fischer for her relentless helpfulness and patience with the making of my poster. I want to thank Adam Jonsson for helping me out with his incredible ingenuity in Photoshop. Finally, I want to give a tremendous eulogy to Sveva Castello at the physics department of Turin University, who spent long nights to find the best possible way of phrasing every sentence and concept, who will forever remain a perpetual source of wonder and curiosity.

References

[1] V. Rajpaul. *A novel algorithm for analysing gravitational microlensing events*. PhD thesis, University of Cape Town, 2012.

[2] A. Udalski. The optical gravitational lensing experiment. real time data analysis systems in the ogle-iii survey. *arXiv preprint astro-ph/0401123*, 2004.

[3] C. Alcock, C. W. Akerlof, R. Allsman, T. Axelrod, D. Bennett, S. Chan, K. Cook, K. Freeman, K. Griest, S. Marshall, et al. Possible gravitational microlensing of a star in the large magellanic cloud. *arXiv preprint astro-ph/9309052*, 1993.

[4] E. . NASA. A horseshoe einstein ring from hubble. Available at `http://apod.nasa.gov/apod/image/1112/lensshoe_hubble_3235.jpg` (2016/23/07).

[5] M. Limousin, J. Richard, E. Jullo, J.-P. Kneib, B. Fort, G. Soucail, Á. Elíasdóttir, P. Natarajan, R. S. Ellis, I. Smail, et al. Combining strong and weak gravitational lensing in abell 1689based on observations obtained at the canada-france-hawaii telescope (cfht). *The Astrophysical Journal*, 668(2):643, 2007.

[6] B. Paczynski. Gravitational microlensing in the local group. *arXiv preprint astro-ph/9604011*, 1996.

[7] R. Di Stefano. Mesolensing explorations of nearby masses: from planets to black holes. *The Astrophysical Journal*, 684(1):59, 2008.

[8] M. S. Andrzej Udalski and S. Kozlowski. Ogle-iv: Fourth phase of the optical gravitational lensing experiment. Available at `http://ogle.astrouw.edu.pl/ogle4/ews/ews.html` (2016/21/07).

[9] D. Bennett, A. C. Becker, J. Quinn, A. Tomaney, C. Alcock, R. Allsman, D. R. Alves, T. Axelrod, J. Calitz, K. H. Cook, et al. Gravitational microlensing events due to stellar-mass black holesbased in part on observations from nasa's hubble space telescope. *The Astrophysical Journal*, 579(2):639, 2002.

[10] C. Henderson, H. Park, T. Sumi, A. Udalski, A. Gould, Y. Tsapras, C. Han, B. Gaudi, V. Bozza, F. Abe, et al. Candidate gravitational microlensing events for future direct lens imaging. *The Astrophysical Journal*, 794(1):71, 2014.

[11] S. A. D. Center. Cds x-match service. Available at `http://cdsxmatch.u-strasbg.fr/xmatch`(2016/12/11).

[12] M. D. Zacharias N. Naval observatory merged astrometric dataset. Available at `http://cdsarc.u-strasbg.fr/viz-bin/Cat?I%2F297`(2016/12/11).

[13] S. A. D. Center. Vizier catalog service. Available at `http://vizier.u-strasbg.fr/viz-bin/VizieR` (2016/21/07).

[14] R. D. Stefano and A. A. Esin. Blending of light in gravitational microlensing events. *The Astrophysical Journal Letters*, 448(1):L1, 1995.

[15] C. Alcock, R. Allsman, D. Alves, T. Axelrod, D. Bennett, K. Cook, K. Freeman, K. Griest, J. Guern, M. Lehner, et al. First observation of parallax in a gravitational microlensing event. *The Astrophysical Journal Letters*, 454(2):L125, 1995.

[16] F. C. Anderson E. Extended hipparcos compilation: Xhip v/137d/xhip. Available at `http://cdsarc.u-strasbg.fr/viz-bin/Cat?V/137D` (2016/29/11).

[17] E. Anderson and C. Francis. Xhip: An extended hipparcos compilation. *Astronomy Letters*, 38(5):331–346, 2012.

[18] S. Rahvar, M. Moniez, R. Ansari, and O. Perdereau. Study of a strategy for parallax microlensing detection towards the magellanic clouds. *Astronomy & Astrophysics*, 412(1):81–90, 2003.

[19] D. Minniti and M. Zoccali. The galactic bulge: a review. *Proceedings of the International Astronomical Union*, 3(S245):323–332, 2007.

[20] B. Gaudi, D. Bennett, A. Udalski, A. Gould, G. Christie, D. Maoz, S. Dong, J. McCormick, M. Szymański, P. Tristram, et al. Discovery of a jupiter/saturn analog with gravitational microlensing. *Science*, 319(5865):927–930, 2008.

[21] A. Gould. Probing machos toward the galactic bulge. *The Astrophysical Journal*, 630(2):887, 2005.

Appendices

Appendix A

Event	**RA**	**Dec**	t_0	t_E	I_0	u_0	f_{bl}
OGLE-2002-BLG-334	18:00:20.29	-32:15:10.6	2452698.967	202.509	16.194	0.150	0.265
OGLE-2005-BLG-36	18:11:29.35	-25:38:24.4	2453540.948	181.532	18.667	0.402	1.00
OGLE-2006-BLG-230	17:59:03.57	-27:16:17.5	2453947.541	179.41	17.932	0.245	0.139
OGLE-2008-BLG-51	18:04:43.62	-28:10:16.7	2454630.427	286.473	16.444	0.367	0.06
OGLE-2011-BLG-64	18:02:57.03	-27:52:52.2	2455751.37	144.212	16.09	1.49	1.00
OGLE-2011-BLG-1349	17:35:55.33	-28:28:12.1	2455811.574	276.078	16.026	0.116	0.076
OGLE-2013-BLG-1831	17:47:33.60	-23:11:08.8	2456581.675	146.868	19.145	0.723	1.00
OGLE-2014-BLG-1159	18:12:17.78	-26:13:27.9	2456895.543	249.277	18.644	0.236	0.122
OGLE-2015-BLG-74	17:53:08.20	-33:12:16.6	2457064.394	141.152	19.367	0.024	0.057
OGLE-2015-BLG-539	17:51:08.04	-36:02:22.1	2457075.234	152.742	18.339	0.103	0.25
OGLE-2015-BLG-1493	17:54:35.14	-29:37:06.9	2457270.87	210.945	18.491	0.046	0.078
OGLE-2016-BLG-443	17:50:10.17	-32:45:39.4	2457544.561	190.627	19.187	0.019	0.591
OGLE-2016-BLG-749	17:42:30.36	-27:15:13.1	2457507.615	168.690	20.351	0.000	0.121

Table 3: Summary table of the original OGLE values for the sample events, with the five PSPL parameters listed. Right Ascension (RA) and Declination (Dec) are in J2000.

Appendix B

Example (1) of source code: the algorithm describing the PSPL model, where the the *automation* algorithm is imported to automatically retrieve data from the online OGLE Early Warning System database.

```
import math
import random
import numpy as np
import automation

#user input
event_year = 2015
event_number = 1493

#### program
data_dir, param_dir = automation.init_automation(year=event_year,event=event_number)
full_param = automation.processparams(year=event_year,event=event_number)
print event_year,event_number
timestart = time.time()

#------------------- open a read file (input data) -----------------
obs_data = open(data_dir,'r')
new_file = str('C:/Users/Elias/Documents/lensing/research/chisq_lists_pspl/chisq_' +
    str(event_year) + '_' + str(event_number) + '.txt')
write_file = open(new_file,'w')

#I. import lightcurve data

time_obs = []
magnitude_obs = []
uncertainty_obs = []

with open(data_dir, "r") as f:
```

```
    for line in f:
        linesplit = line.split(" ")
        time_obs.append(linesplit[0])
        time_obs = map(float, time_obs)
        magnitude_obs.append(linesplit[1])
        uncertainty_obs.append(linesplit[2])
        magnitude_obs = map(float, magnitude_obs)
        uncertainty_obs = map(float, uncertainty_obs)
event_year = str(event_year)

#II. Set up Initial Data for PSPL Fit

#param_arr = [t0,tE,Ibl,u0,fbl,theta,v_transverse]
param_arr = [full_param[2],full_param[9],full_param[7], full_param[3], full_param[6]]
print "Initial Parameters [t0,tE,Ibl,u0,fbl]:" + str(param_arr)

#set up time
t_start=time_obs[0]
t_end=time_obs[-1]

#III. Chi-square minimization algorithm
#A. define variables for algorithm
r=0
n=0
i=0
iterations = 1000 #max number of iterations
chisqr=0          #initialize chi square
total_arr = []    #list to hold good parameters from algorithm
chisqr_arr = []   #list to hold good chi square values
lowchi = 1000
total_chi_arr = [lowchi]


#B. start the chisquare algorithm
print "Starting the Chi-Square Minimization Algorithm...\n"
```

```python
while r < 1:
    i+=1
    t0 = np.random.normal(param_arr[0],2)
    tE = np.random.normal(param_arr[1],5)
    Ibl = np.random.normal(param_arr[2],.1)
    u0 = np.random.normal(param_arr[3],.1)
    fbl = np.random.normal(param_arr[4],.1)
    chisqr=0
    if t0>0 and tE>0 and Ibl and 0<=u0<=2 and 0<fbl<=1:
        for j in range(0,len(time_obs)):
            y_model=[]
            #function for calculating magnitude
            u = np.sqrt(u0**2.+((1./tE)*(time_obs[j]-t0))**2.)
            A = (u**2.+2.)/(u*np.sqrt(u**2.+4.))
            Aobs= fbl*(A-1)+1
            I = Ibl - 2.5*(np.log(Aobs))/(np.log(10)) #convert natural logarithm to base 10
            y_model.append(I)
            d=float(magnitude_obs[j])-I
            e=d/(float(uncertainty_obs[j]))
            e=e**2
            chisqr+=e
        chisqr=chisqr/(len(magnitude_obs)-5)
        if chisqr < lowchi:
            n+=1

            #update parameters and lowest chisquare
            total_chi_arr.append(chisqr)
            param_arr = [t0,tE,Ibl,u0,fbl,chisqr]
            total_arr.append(list(param_arr))
            chisqr_arr.append(chisqr)
            chidiff = lowchi - chisqr
            lowchi = chisqr

            #output the current lowest chi
```

```
            print "Run number "+str(n) + " iterations " + str(i) + " out of " + str(iterations)
            print "Chi-Square: "+str(chisqr)
            print "Parameters: "+str(param_arr)+"\n\n"

            #reset count and restarts
            i=1
    if i>iterations:
        break

#IV. Output results
print "\n\nComplete Chi-squares" + str(total_chi_arr)
print "\n" + str(min(chisqr_arr))

# First writing the model parameters with best chisq:
write_file.write('Best parameters and chi [t0,tE,Ibl,u0,fbl,chisqr]: ' + str(total_arr[-1]) + '\n\n' + 'Other values:' + '\n')

#then adding all the models to write_file (for analyzing all chisq values):
for item in total_arr:
    write_file.write("%s\n" % item)

obs_data.close()
write_file.close()
```

Example (2) of source code: the algorithm describing the parallax model, where the *perihelion* algorithm aims to match each event with occuring perihelion (in Heliocentric Julian Dates (HJD)) that year. The separate *ecliptic converter and tc* program, based on the *astropy* package (available on `http://www.astropy.org/`), converts the equatorial coordinates (OGLE standard) to ecliptic to facilitate calculation, and finds the time of Earth's closest approach to sun-source line.

```python
from __future__ import division
from math import *
import numpy as np
from numpy import matrix
from numpy import linalg
import pylab as pl
from decimal import Decimal
import operator
import time
from ecliptic_converter_and_tc import tc,eq2ec
import automation

#user input
event_year = 2015
event_number = 74

#### program
data_dir, param_dir = automation.init_automation(year=event_year,event=event_number)
full_param = automation.processparams(year=event_year,event=event_number)
print event_year,event_number
timestart = time.time()

#open a read file (input data)
# ---------------------------------------------------

obs_data = open(data_dir,'r')
new_file =
```

```
    str('C:/Users/Elias/Documents/lensing/research/chisq_lists_parallax/chisq_' +
    str(event_year) + '_' + str(event_number) + '.txt')
write_file = open(new_file,'w')

#I. import lightcurve data

time_obs = []
magnitude_obs = []
uncertainty_obs = []

with open(data_dir, "r") as f:
    for line in f:
        linesplit = line.split(" ")
        time_obs.append(linesplit[0])
        time_obs = map(float, time_obs)
        magnitude_obs.append(linesplit[1])
        uncertainty_obs.append(linesplit[2])
        magnitude_obs = map(float, magnitude_obs)
        uncertainty_obs = map(float, uncertainty_obs)
event_year = str(event_year)

#II. Set up Initial Data for Parallax Fit

#perihelion times (tp) from 2002-2016
#retrieved from http://www.astropixels.com/ephemeris/perap2001.html
#converted to Heliocentric Julian Dates (HJD) with https://www.aavso.org/jd-calculator
tp_arr = [2452277.08958, 2452643.70972, 2453009.23750, 2453372.52431, 2453740.14583,
    2454104.32153, 2454468.49375, 2454836.14583, 2455199.50625,
    2455565.27222,2455931.52222,2456294.69306,2456661.99931,2457026.77500,
    2457390.45069]

#ecliptic latitude (converter from equatorial)
beta = eq2ec(full_param[0],full_param[1],8,"spherical")[1]
print "\nBeta: " + str(beta)

```

```
#time of perihelion
if int(event_year) < 2017 and int(event_year) > 2001:
    difference = int(event_year) - 2002
tp = tp_arr[difference]
print "T_p:" + str(tp)

#time of closest approach to sun-source line
t_c = tc(full_param[0],full_param[1],8,tp_arr[difference])
t_c = float(t_c)

print "T_c: " + str(t_c)
#param_arr = [t0,tE,Ibl,u0,fbl,theta,v_transverse]
param_arr = [full_param[2],full_param[9],full_param[7], full_param[3], full_param[6]]
#theta angle
param_arr.append(0)
#add in v_transverse as 31.06875 km/s (using mean from XHIP v_transverse)
param_arr.append(31.06875)
print "Initial Parameters [t0,tE,Ibl,u0,fbl,theta,v_transverse]:" + str(param_arr)

#set up time
t_start=time_obs[0]
t_end=time_obs[-1]

#III. Chi-square minimization algorithm

#A. define variables for algorithm
r=0
n=0
i=0
iterations = 1000 #max number of iterations
chisqr=0          #initialize chi square
total_arr = []    #list to hold good parameters from algorithm
chisqr_arr = []   #list to hold good chi square values
lowchi = 1000
total_chi_arr = [lowchi]
```

```
ohm_0 = 2*pi/365
epsilon = 0.017   #Earth's orbital eccentricity

#C. start the chisquare algorithm
print "Starting the Chi-Square Minimization Algorithm...\n"
while r < 1:
    i+=1
    t0 = np.random.normal(param_arr[0],2)
    tE = np.random.normal(param_arr[1],5)
    Ibl = np.random.normal(param_arr[2],.1)
    u0 = np.random.normal(param_arr[3],.1)
    fbl = np.random.normal(param_arr[4],.1)
    theta = np.random.normal(param_arr[5],2*pi)
    #v_transverse data taken from XHIP V/137D/XHIP, fit density using R with lognormal
    v_transverse = np.random.lognormal(3.146258269,0.801087731)

    chisqr=0
    if t0>0 and tE>0 and Ibl and 0<=u0<=2 and 0<fbl<=1 and v_transverse>0:
        for j in range(0,len(time_obs)):
            y_model=[]
            x = (time_obs[j]-t0)/tE
            #Einstein radius projected onto the observer (sun) plane
            radius = (2/(v_transverse*tE))*(1-(epsilon*cos(ohm_0*(time_obs[j]-tp))))
            #inter_ohm = ohm(t-tc)
            inter_ohm =
                (ohm_0*(time_obs[j]-t_c))+(2*epsilon*sin(ohm_0*(time_obs[j]-tp)))
            ##calculation of u**2 divided into seperate terms
            term1 = (u0**2)+(x**2)+((radius**2)*((sin(inter_ohm))**2))
            term2 = 2*radius*sin(inter_ohm)*(x*sin(theta)+u0*cos(theta))
            term3 = (radius**2)*((sin(beta))**2)*((cos(inter_ohm))**2)
            term4 = 2*radius*sin(beta)*cos(inter_ohm)*((x*cos(theta))-(u0*sin(theta)))
            u_squared = term1+term2+term3+term4
            u = sqrt(u_squared)
            A = (u**2+2)/(u*((u**2+4)**0.5))
            A_obs = (fbl)*(A-1)+1
```

```
            I =(Ibl)-2.5*(np.log(A_obs))/(np.log(10))
            y_model.append(I)
            d=float(magnitude_obs[j])-I
            e=d/(float(uncertainty_obs[j]))
            e=e**2
            chisqr+=e
        chisqr=chisqr/(len(magnitude_obs)-7)
        if chisqr < lowchi:
            n+=1

            #update parameters and lowest chisquare
            total_chi_arr.append(chisqr)
            param_arr = [t0,tE,Ibl,u0,fbl,theta,v_transverse,chisqr]
            total_arr.append(list(param_arr))
            chisqr_arr.append(chisqr)
            chidiff = lowchi - chisqr
            lowchi = chisqr

            #output the current lowest chi
            print "Run number "+str(n) + " iterations " + str(i) + " out of " + str(iterations)
            print "Chi-Square: "+str(chisqr)
            print "Parameters: "+str(param_arr)+"\n\n"

            #reset count and restarts
            i=1
    if i>iterations:
        break

#IV. Output results

print "\n\nComplete Chi-squares" + str(total_chi_arr)

print "\n" + str(min(chisqr_arr))
chisqr_arr.sort()
```

```
sorted_lst = []
for chisqr in chisqr_arr:
    for i in range(len(total_arr)):
        if chisqr == total_arr[i][7]:
            sorted_lst.append(total_arr[i])
            print total_arr[i]
#print time.time() - timestart

#First writing the model parameters with best chisq:
write_file.write(’Best parameters and chi [t0,tE,Ibl,u0,fbl,theta,v_transverse,chisqr]: ’ + str(total_arr[-1]) + ’\n\n’ + ’Other values:’ + ’\n’)

#then adding all the models to write_file (for analyzing all chisq):
for item in total_arr:
    write_file.write("%s\n" % item)

obs_data.close()
write_file.close()
```